이학박사 학위논문

전자파 변조를 위한 제로 나노미터 갭 기술 개발

Development of Zero-Nanometer Gap Technology for Electromagnetic Wave Modulation

2022 년 02 월

서울대학교 대학원

물리천문학부

Bamadev Das (바마대브)

Development of Zero-Nanometer Gap Technology for Electromagnetic Wave Modulation

지도교수 홍성철

이 논문을 이학박사 학위논문으로 제출함
2022 년 02 월

서울대학교 대학원
물리천문학부

Bamadev Das (바마대브)

바마대브의 (**Bamadev Das**) 박사 학위논문을 인준함

2022 년 02 월

위 원 장 차국린 (인)

부 위 원 장 홍성철 (인)

위 원 전헌수 (인)

위 원 이탁희 (인)

위 원 정지윤 (인)

Abstract

In this thesis, I demonstrated a new concept of sample which allows the full control of light i.e. from transparency to full extinction of the wave. To demonstrate this, I fabricated two kinds of sample i.e. closable nanotrench and zero-nanometer-gap. These samples are fabricated on a flexible substrate using atomic layer lithography. Taking advantage of the flexible substrate, samples are applied with mechanical strain to control the width of the gap, which manipulates the light. When an inward bending is applied to closable nanotrench, the transmission decreases drastically and becomes zero in microwave (12-18 GHz) and terahertz (0.2-2 THz) frequencies. which shows a subwavelength scale closing of nanogap. This decrease in transmission is understood by R-C modeling and structural mechanics simulation. Using a high-density closable nanotrench sample, the full modulation of microwave transmission is also achieved. By applying an outward bending to zero-gap sample, the transmitted intensity increases from 0.01% to 75%. As an application, zero-gap sample is used as a transformative metasurface, in which it transforms from mirror to polarizer with bending. In terms of stability, it is found that the zero-gap's function remain stable for more 10,000 times of bending and relaxation cycle, better than closable nanotrench which could sustain till 200 times of bending cycles.

KEYWORDS: Closable nanotrench, zero-nanometer-gap, terahertz, microwave, transformative metasurface, polarizer

Student Number: 2016-39035

Contents

List of Figures

Lists of tables

Chapter 1.

Introduction

1.1 Background

Nano-optics or nano-photonics describes an active and strongly developing research field that involves the interaction of light with matter at nanometer length scale [1-3]. The interaction of light with metal pattern such as hole, grating etc. is one of the most studied research field in this context, where unprecedented phenomenon is observed. Hole in a metal film is the simplest nanostructure to study the light interaction with it. The light transmission through such perforated metal films has been researched empirically since middle ages. It was shown by Bethe that a circular hole with diameter in subwavelength scale transmits a part of incident energy i.e. $T = 0.24\left(\frac{r}{\lambda}\right)^4$ [4-6]. This shows a weak optical transmission which became issues for different applications such miniaturization of optical components that could be used for modern tools beyond diffraction limit. During late twentieth century, the discovery of extraordinary transmission through periodic subwavelength holes in metal film by Ebbesen revolutionize the field of optics because it showed to have transmitted orders of magnitude more than the intensity predicted by Bethe's equation through the holes [7-8].

Currently, the term extra ordinary transmission is more generalized which referred to the enhanced transmission in different kind of systems such as circular hole or rectangular hole which are isolated or arranged periodically, or randomly distributed. In fact, the

extraordinary optical transmission is observed in different frequency regime such as optical, terahertz and microwave frequencies [9].

The extraordinary transmission observed by Ebbesen is the result of the coupling of incident electromagnetic wave to the surface modes residing in the interface between the substrate and the metal holes [7]. This transmission is observed in visible and near infrared frequency regime. The mechanism of transmission of electromagnetic in long wavelength such as microwave and terahertz is different as these frequencies cannot excite surface plasmon in the metal. The details of the mechanism in these frequencies regime is described in the next section.

1.2 Terahertz and Microwave Funneling in Nanoslit and Field Enhancement

With advancement of nanotechnology, it is possible to fabricate sample with different dimension. This allows researcher to study different mechanism in different wavelength scale. The extraordinary transmission in terahertz frequency is also observed in nanoslit or nanoslot antenna [10-12]. However, in this frequency the transmission is governed by capacitive coupling of the antenna with the incident terahertz wave as shown in Figure 1.1. When terahertz electromagnetic wave is impinged on the nanoslit antenna, it introduces a surface current in the metal due to the magnetic component of the field. Due to this surface current, the charges flows and gets accumulated at the Sommerfeld half plane as shown in Figure 1.1. Hence the gap acts as a capacitor which transmits the wave.

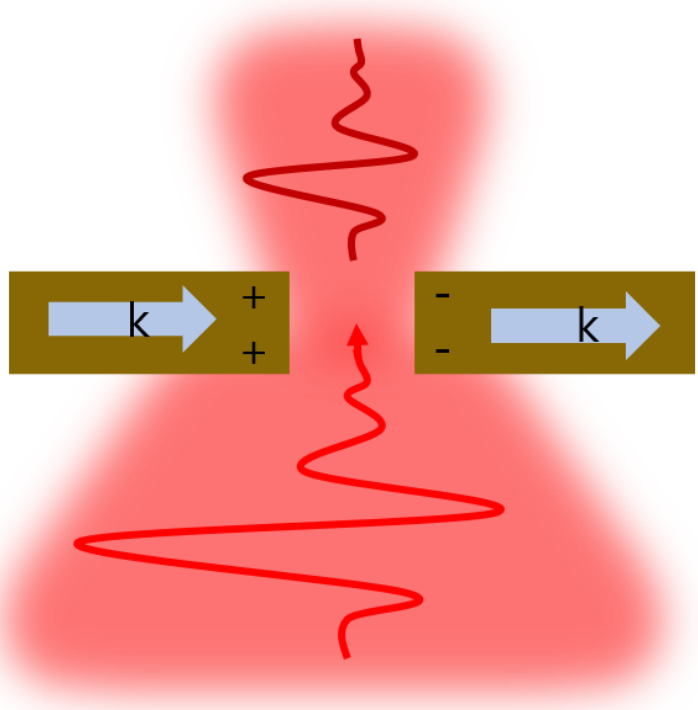

Figure 1.1. Schematic diagram describing the terahertz transmission through nanoslit antenna via capacitive charging of the gap. Schematic diagram describing the terahertz transmission through nanoslit antenna via capacitive charging of the gap

This similar phenomenon is also demonstrated microwave frequency, where almost 50% of transmittance is achieved in 12-40 GHz frequency band width [13-14]. One of the feature of nanoslit is the huge field enhancement and field confinement in the gap region [10]. This field enhancement is important due to its applications such as optical component, sub-wavelength lithography, sensing etc. [15-19]. Seo et al. demonstrated a field enhancement of 1000 inside the nanoslit of gap width 70 nm, which is 30000 times smaller than the wavelength [10]. The origin of this field enhancement is from the charge accumulation around the slit edges which are induced by oscillating current impinging on the metal film [13-14]. Since the attraction or field between the charges inside the metal gap is responsible for this enhancement transmission (i.e. field enhancement), it can be increased if we decrease the gap width. With significant improvement in nanotechnology, samples containing nanoslits of width ~1 nm is possible to fabricate [11,14]. A nanoslit with 1 nm width is reported to have ~10000 field enhancement in terahertz frequencies. A huge field enhancement of ~4500 in microwave frequency is also reported in such sample which are customized for such frequency [20].

So clearly, gap width is important to achieve a certain amount of field enhancement. In fact, samples with very small gap width in the order of sub-nanometer scale is desirable due to its strong electric field enhancement. In this regard, a detailed experimental demonstration and theoretical explanation of increase in field enhancement with decrease gap width is reported in [13-14].

When it comes feature size of the metasurface, the advancement of nanotechnology has

made it possible to achieve sub-nanometer length where a 0.3 nm van der Waals gap is achieved by using graphene as a spacer in between two metals [21]. A detailed feature size vs year [22-32] is presented in figure 1.2. However, controlling the gap width from micron to nanometer scale still remain a challenge from technological point of view. One of the purpose of having the ability to control the gap width is to manipulate the interaction of electromagnetic wave actively without changing the sample as a whole. In order to understand the active control of electromagnetic wave, we did some literature survey which are written in the next section.

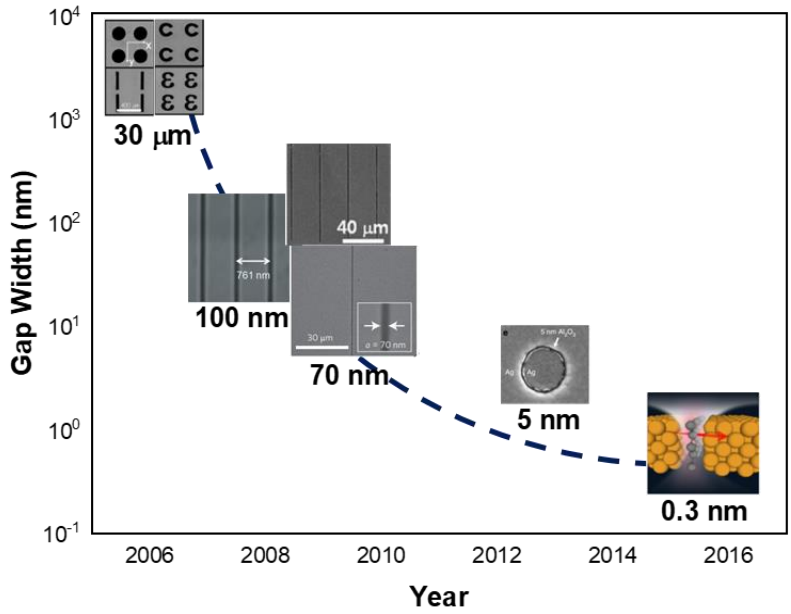

Figure 1.2. Development of smaller feature size with nanotechnology advancement. Feature size of sample with respect to year. Size of the gap in the sample increase with the advancement of the nanotechnology.

1.3 Active Control of Electromagnetic Wave

There are various methodologies reported to control electromagnetic wave using metasurfaces. Broadly, these methodologies can be categorized into four types which are (a) integration of functional materials with metasurface, (b) using thermal energy, (c) break-junction, (d) mechanical strain. In the first method, researchers usually metasurface made with functional materials or metal nanostructure patterned on thin film of functional materials. By controlling the properties of the materials, one could manipulate the electromagnetic response in certain frequencies [33-34]. However, one has to choose right kind of materials to integrate with metasurface because of fabrication issues. Moreover, even though the functional is integrated, the electromagnetic response couldn't be control fully, say from 100% transmission to zero transmission. For the second method, thermal energy can be used for electromagnetic manipulation. Yun et. al. [35] reported about the thermal energy controlling electromagnetic response from a nanoslit antenna. In this case, it requires a high temperature to achieve a small amount of control of waves. Again, the thermal energy couldn't control the electromagnetic field response fully. A third type of control is the use break-junction. In this case, one needs to design certain kind of meta-structure to be used as break-junction type. Rhie et.al. reported recently about the control of THz wave by using a bowtie antenna [36]. A bowtie was fabricated which got special notch structure in the middle. This notch allows to propagate a crack when the sample bent. This break-junction type sample cannot be extended to big thinfilm where one can have slits by cracking the film. Final one is the direct mechanical stretching of the metasurface. The mechanical stretching of the

metasurface changes overall dimension of the sample, thereby enabling the control over the electromagnetic response. However, till date reported papers have shown that it needs huge strain such 50% or more to achieve minor modulation of depth [35-36].

1.4 Purpose of Research

So in this thesis, I did research on gap-width control to manipulate the electromagnetic response from an array of slits fabricated on flexible substrates. Full modulation of electromagnetic wave by controlling the gap width is demonstrated by using two different samples i.e. (a) closable nanotrench and (b) zero-nanometer gap (zero-gap). Closable nanotrench contain array of nanoslits with gap width 20nm, which become zero-nm with the application of external mechanical inward strain. This allows to have full control over electromagnetic response. Zero-nanometer-gap sample behaves as a thin film. However, with external outward bending, array of slits is cracked opened to have a maximum transmission through the sample.

Chapter 2.

Optical Zero-Nanometer Gap by Closable Nanotrench

2.1. Introduction

Active control of metamaterials has been in the focus of researchers because of its potential device applications such as super-lensing, cloaking, optical transparency and so on. In electromagnetism, the functionality of materials depends on permittivity and permeability. By controlling these two fundamental parameter, one can dynamically change the functions of a metamaterials. Alteration of metamaterial's geometrical parameter or unit cell by external mechanical strain is a direct and simple way of controlling the properties of the sample [37-41].

In this chapter, I used a slit structure containing nanogap (metal-air-metal gap) named "closable nanotrench" to demonstrate the dynamic behaviors of the sample, as shown Figure 2.1. As shown in the figure, the closable nanotrench is fabricated on top of polyethylene terephthalate (PET) substrate. Taking advantage of the substrate, the sample is bent, which eventually closed nanogap in the sample (hence named closable nanotrench). A detailed fabrication methodology is explained in the next section.

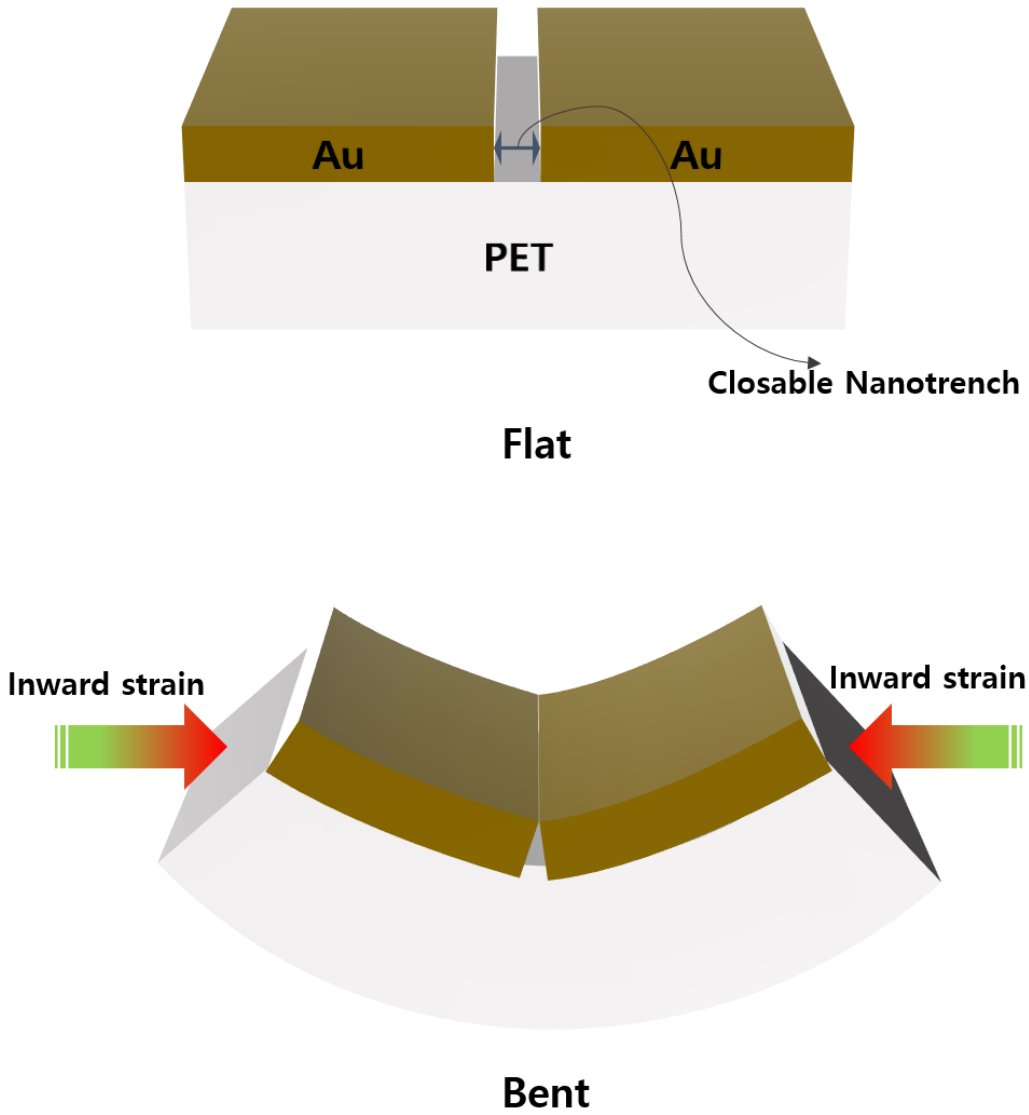

Figure 2.1. Schematic diagram of a typical closable nanotrench at flat and bent. Top schematic diagram shows a single closable nanotrench which is a metal-air-metal long slit structure fabricated on top of PET substrate. Bottom schematic diagram represents the nanotrench in a bent state due to inward strain applied to the sample.

2.2. Fabrication and Characterization of Closable Nanotrench

The detailed fabrication of closable nanotrench is shown schematically in Figure 2.2. The fabrication process which is called "atomic layer lithography" is reported elsewhere [11, 42-43]. At first, PET substrate having 250 μm thick is cleaned by using acetone and isopropanol (IPA) for 5 min in ultrasonic. Image reversal photoresist (AZ5214E) is then spin-coated on PET at 4000 RPM for 60 seconds. After this, the resist is baked at 95 ^{0}C for 60 seconds in hot plate. The height of photoresist thinfilm is about ~1.45 μm. The resist thin film is exposed with ultraviolet light of energy 62 mJ/cm^2 (center wavelength 364 nm) under photomask that contains desired pattern. To achieve image reversal, the resist is baked again at 115 ^{0}C for 90 seconds, followed by a flood exposure of ultraviolet light of dose 210 mJ/cm^2. Finally, the patters are developed using MIF300 developer solution and the sample is ready for metallization. Three nanometer thick titanium and 150 nm thickness of gold (Au) is deposited onto the sample using E-beam evaporator. The photoresist is then lifted off by using acetone to get the desired 1st layer metal pattern, shown in Figure 2.2(a). Then, alumina (Al_2O_3) of thickness 20nm is deposited conformally on 1st layer metal using atomic layer deposition (Figure 2.2(b)). The second Au metal of 150 nm thickness is again plugged in by E-beam evaporator to create a gap between the metal layer, in which alumina acts as a spacer (Figure 2.2(c)). The excess metal on top is mechanically exfoliated by using scotch tape, making the sample surface plane (Figure 2.2(d)). To make metal-air-metal, the gap materials i.e. alumina is etched away [44] by dipping the sample in one mole of KOH solution for 20 min (Figure 2.2(e)). Finally, the sample "closable nanotrench" is ready for different experiments (Figure 2.2(f)).

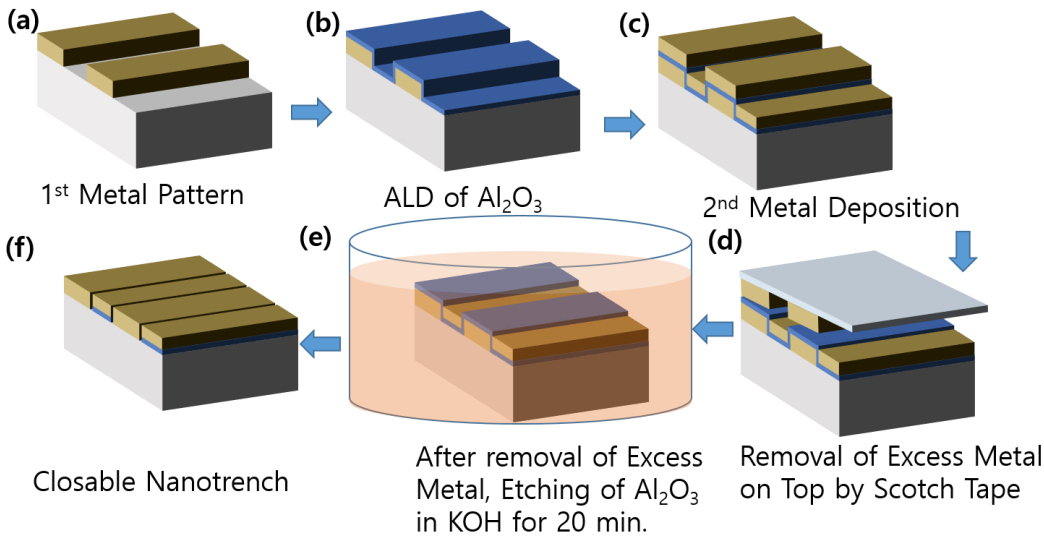

Figure 2.2. Schematic diagram of fabrication process of closable nanotrench. (a) 1st layer gold metal pattern on PET using standard lithography and lift off process. (b) Atomic layer deposition of alumina of 20 nm thickness, which acts as a spacer in further gap fabrication. (c) Second gold metal deposition which finally create the gap. (d) Tapping of excess metal using scotch tape to make the sample plane. (e) Etching gap materials i.e. alumina using KOH solution. (f) Final device after etching gap materials to create metal-air-metal gap, which is called closable nanotrench.

The fabricated closable nanotrench sample is characterized by field emission scanning electron microscopy (FESEM) imaging. By using atomic layer lithography, I could fabricate the sample in wafer-scale, as shown in digital photograph in Figure 2.3. (a). The typical size of sample is 20 mm by 20 mm. This sample size is useful and judiciously fabricated to have better compatibility with experimental setup while measuring in long-wavelength regime such as microwave and terahertz. It contains an array of closable nanotrench of width 20 nm, height 150 nm with length 20 mm. Shown in Figure 2.3. (b) is the top view of closable nanotrenches array structure having periodicity of 200 μm. The cross-sectional FESEM image of a closable nanotrench is shown in Figure 2.3. (c). The image confirms the fabrication of a good quality nanotrench width of ~20 nm with height 150 nm.

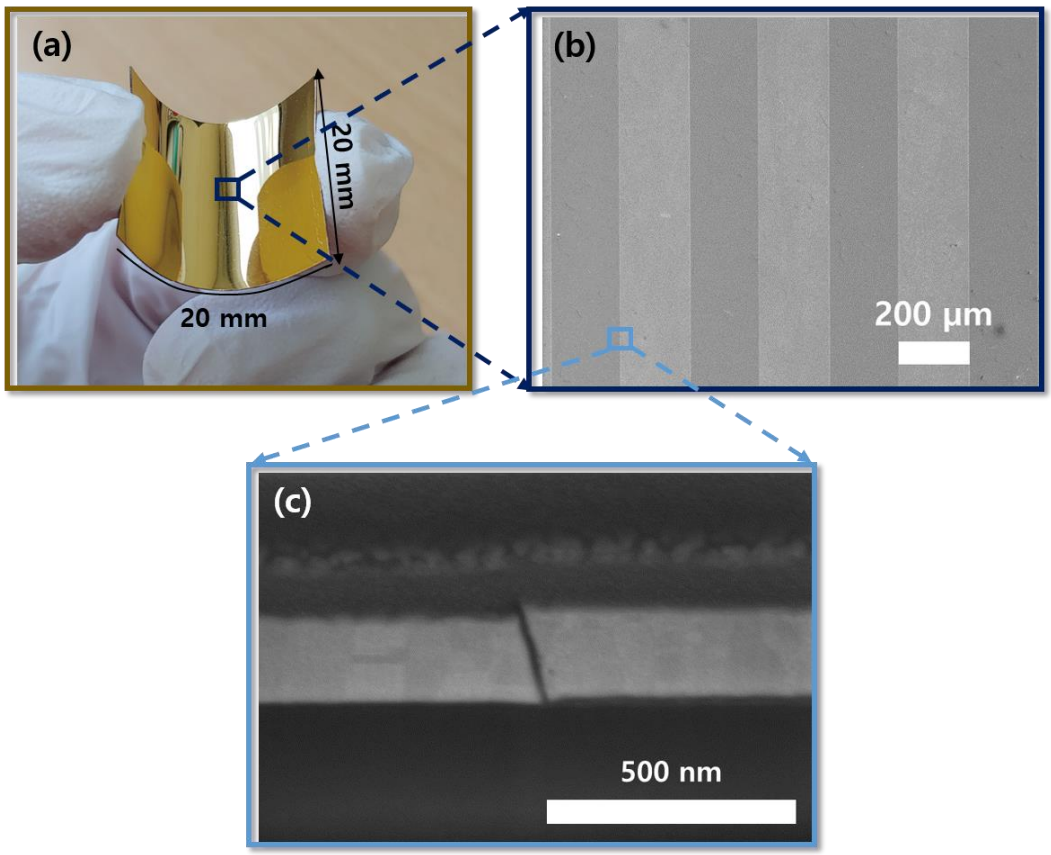

Figure 2.3. Imaging of fabricated closable nanotrench. (a) Digital image of sample. The typical size of the sample is 20 mm by 20mm. (b) Top view FESEM image of an array of closable nanotrenches with a periodicity of 200 µm. (c) Cross-sectional FESEM image of single closable nanotrench, showing ~20 nm width and ~150 nm height.

2.3. Microwave Transmission Through Closable Nanotrenches

Microwave transmission in closable nanotrenches sample is measured by using a pair of open-ended waveguide connected to a vector network analyzer (VNA) [13]. The spot-size of this waveguide is 15.88 mm by 7.9 mm, which is why the fabricated sample size is 20 mm by 20mm. The detail description of this measurement method is explain in Appendix 5.1. The sample (nanotrench width 20 nm, height 150 nm) shows approximately 50% of transmission (Figure 2.4.) when the long axis of the nanotrench is perpendicular to the polarization of electric field. When the electric field polarization is perpendicular to axis of gap (p-polarized; see inset of Figure 2.4.), the gap is charged up due to the magnetic field component which is parallel to the metal film, which eventually behaves as a capacitor, offering high transmitted amplitude. In order to confirm the capacitive coupling of gap to the electromagnetic wave, the transmission through the gap, when the electric field polarization is parallel (s-polarized; see inset of Figure 2.4.),), is also measured and it shows almost zero transmission through the sample (Figure 2.4.).

To check the functionality of the closable nanotrench, the sample is applied with inward strain while measuring microwave transmission. The sample is put in between the waveguide and bent using a custom made sample holder to measure the transmission at bent condition. The measuring technique and strain application using a sample holder is explained in Appendix 5.1. One of the important parameter in this experiment is bending radius of curvature (r_c). Bending radius of curvature determine the output of the sample functions. Hence calculation of this parameter is vital.

The radius of curvature can be calculated using the following general equation.

$$r_c = \left|\frac{(1+y'^2)^{3/2}}{y''}\right| \quad \text{----------(1.1)}$$

Where y represents the function of the curved PET substrate. In this case, the bent substrate is assumed to be $y = a\sin(kx)$. By using appropriate boundary condition, the radius of curvature is found out to be

$$r_c = \frac{L^2}{\pi^2 A} \quad \text{----------(1.2)}$$

Where L is the length of bent substrate. The calculation of this equation is given in Appendix 5.3.

Figure 2.5. represents the measured microwave transmitted amplitude in closable nanotrench with respect to bending radius of curvature ranging from flat to r_c = 11.06 mm. At first, the sample is inserted in between two waveguides and bent gradually by using a custom sample holder capable of applying strain to check the microwave transmission, as shown in Figure 2.5. (a). The transmitted amplitude in closable nanotrench with respect to bending radius of curvature is presented in Figure 2.5. (b). At flat, the closable nanotrench sample transmits ~50% of broad-band microwave amplitude in frequency bandwidth 12-18 GHz. Note that, the transmitted amplitude is directly related to gap width of the nanotrench. As the sample is bent, the transmission is also decreased. As the transmission is due to the capacitive coupling with gap, it needs a sub-wavelength scale of reduction in gap width to achieve a certain decrease in transmitted amplitude [34].

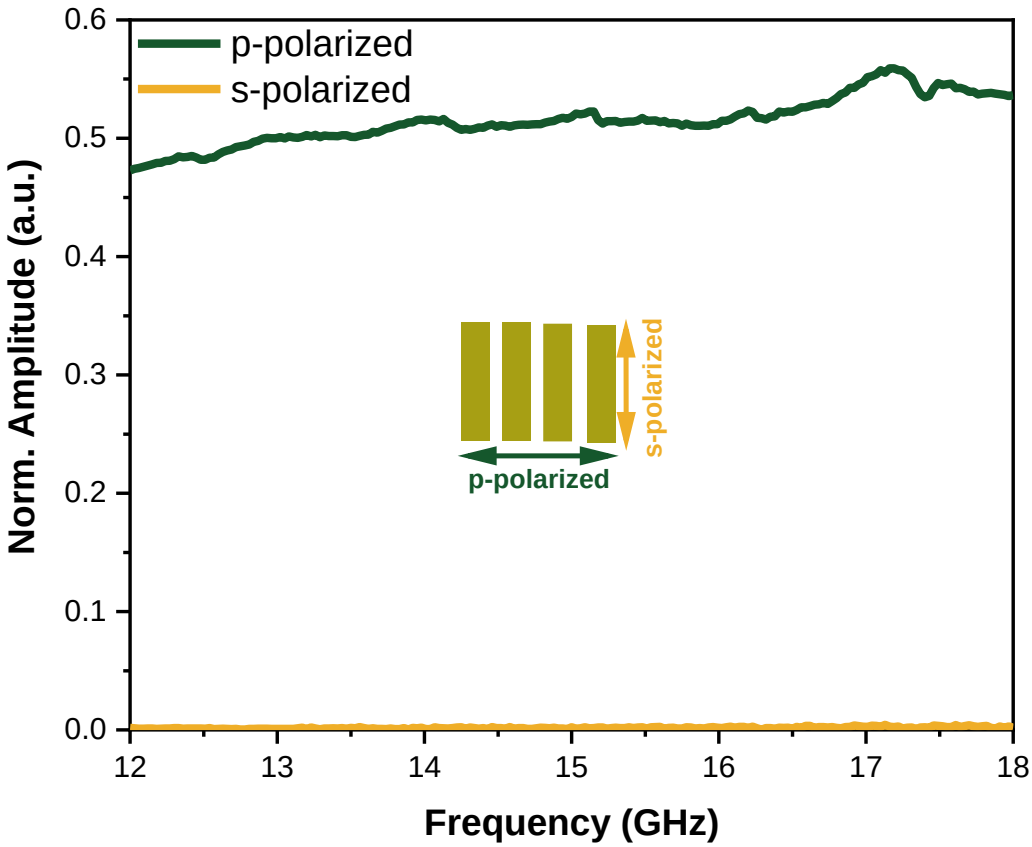

Figure 2.4. Microwave transmission through closable nanotrenches sample. Measured transmission through closable nanotrenches with 20 nm width and 150 nm height when the nanotrench long axis is perpendicular (p-polarized) and parallel (s-polarized) to polarization of electric field.

So with the application of external strain, the nanotrench is closed in a subwavelength scale which ultimately modulates the electromagnetic wave. A perfect extinction of microwave in closable nanotrench is achieved, when the sample is bent with a radius of curvature 11.06 mm as shown in Figure 2.5. (b). This shows the complete collapsing of nanotrench, where metal plates are touch each other to remove the capacitive nature of gap. The normalized amplitude vs curvature $\left(\frac{1}{r_c}\right)$ in Figure 2.5. (c) shows the complete functionality of the closable nanotrench sample where I could achieve perfect extinction of electromagnetic wave with almost 99.9% of modulation of depth.

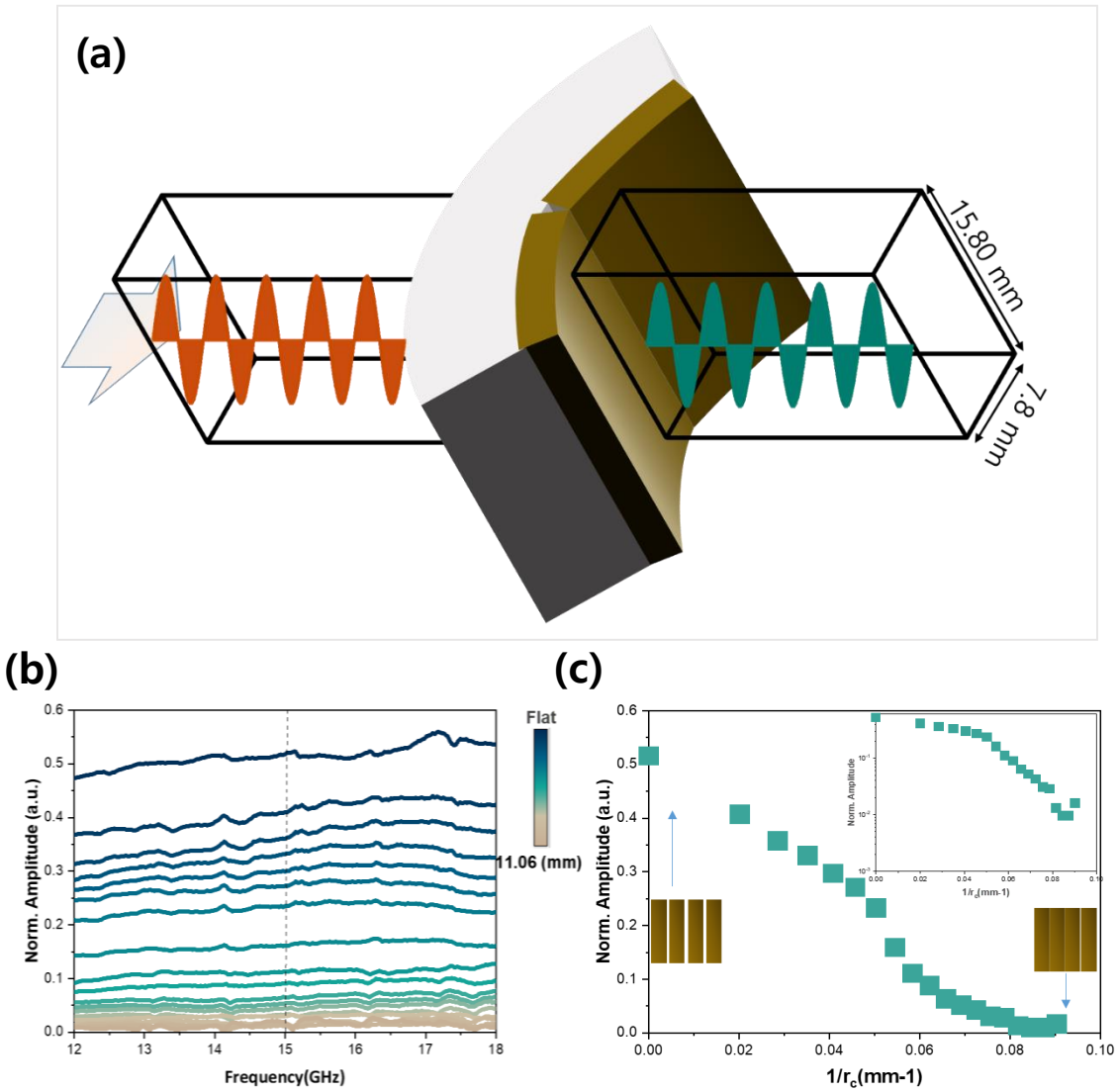

Figure 2.5. Microwave transmitted amplitude with respect to bending radius of curvature. (a) Schematic diagram describing microwave transmission measurement with different bending radius of curvature. (b) Measured microwave transmitted amplitude through closable nanotrench in 12-18 GHz w.r.t. bending radius of curvature. (c) Curvature vs normalized amplitude graph, showing the characteristics of the sample.

2.4. Structural Mechanics Simulation of Closable Nanotrench

In order the understand the perfect extinction of electromagnetic wave in closable nanotrench, firstly the structural mechanics of nanotrench closing is investigated, which is shown in Figure 2.6. (a). As the sample is bent, the substrate at the bottom of nanotrench starts compressing. There is enormous stress generated at the metal-PET interface at the vicinity of nanotrench, which is translated into the top part of the nanotrench, thereby closing the gap in a tapered geometry as shown in Figure 2.6. (a). Figure 2.6. (b) shows the gap at upper part is closing faster than the gap width at the bottom part. In both the part i.e. bottom and top part, the decrease in gap width decreases linearly with bending radius of curvature. The top part of the gap finally touches each other and hence collapsing the capacitive nature of gap.

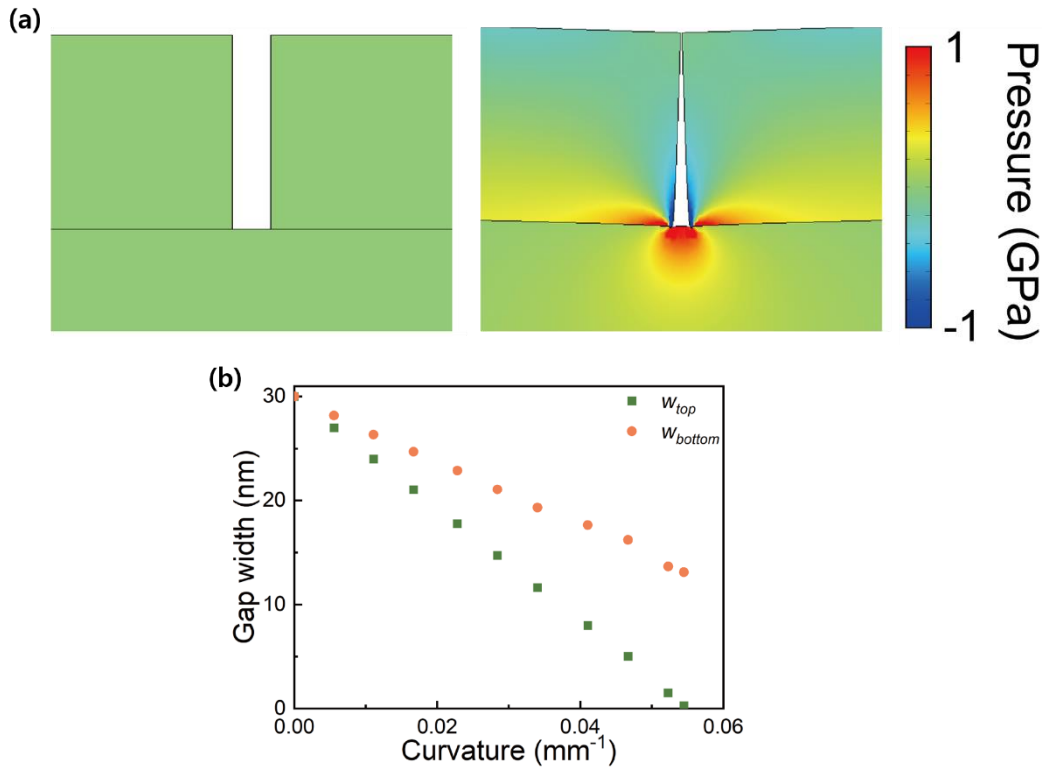

Figure 2.6. Structural simulation of closable nanotrench. (a) Modelling explaining the closing dynamics of closable nanotrench. (b) Gap width vs curvature calculation from simulation of closable nanotrench.

2.5. Terahertz Transmission and Resistor-Capacitor (R-C) Modeling in Closable Nanotrench

To understand the mechanism of closing the nanotrench in the language of circuit theory and plasmonics, the terahertz time domain spectroscopy (THz-TDS) is done [45-46]. One of the important feature of THz-TDS is that we can get phase and amplitude information of transmitted wave through closable nanotrench with each bending curvature condition. The details of THz-TDS setup and measurement scheme are explained in Appendix 5.2. Briefly, the closable nanotrench is inserted in the way of THz propagation as shown in Figure 2.7. (a), to measure THz transmission. At first, the transmitted amplitude at flat condition is measured. The measured transmitted amplitude is about ~10% transmission. As the sample is bent from flat to 20, 16, 9 mm bending radius of curvature, the transmission decreases from ~10% to ~4%, ~1.5% and finally perfect extinctions, as shown in Figure 2.7. (b).

This decrease in transmission can be understood by using circuit theory [44, 47-48]. In this case, resistor-capacitor circuit modelling is done to understand the perfect extinction in the closable nanotrench. At flat, the sample has nanotrench, which perfectly behaves like capacitor as shown in Figure 2.7 (a). However, as the sample is bent, the top part of metal near the vicinity of nanotrench starts touching each other (Figure 2.6. (a)), thereby creating electrical path across the trench. The touching of metal parts destroys the perfect capacitive nature of gap. Hence when the sample is bent, it can be modeled by resistor-capacitor circuit, as shown in Figure 2.7. (a) in bottom schematic diagram.

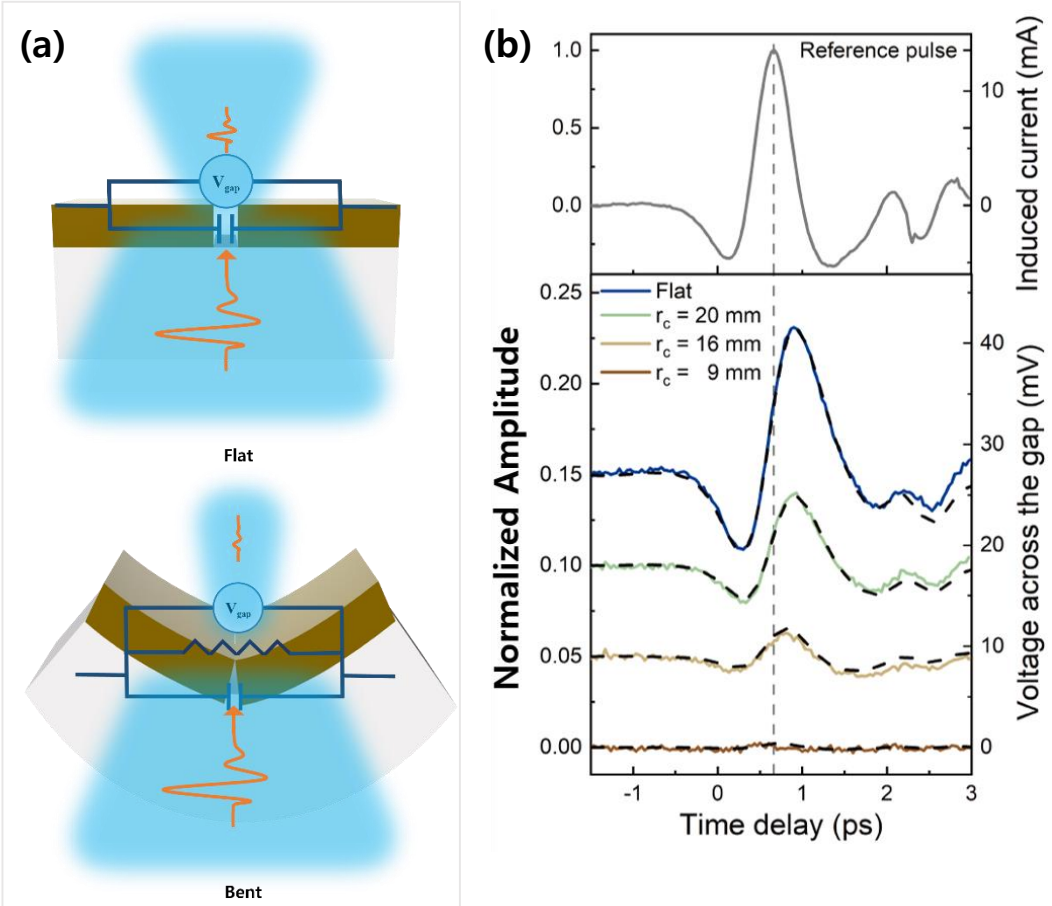

Figure 2.7. THz transmission and resistor-capacitor (R-C) modelling in closable nanotrench. (a) Schematic diagram describing terahertz transmission and R-C modeling in closable nanotrench. (b) Measured THz transmission through closable nanotrench with various bending condition. Calculated voltage developed across the gap is also mentioned in the y-axis of the graph. Dashed lines are the fitted curve with R-C modelling.

The incident THz wave induces surface current in the metal surface. This induced current density is calculated from incident THz pulse by $I_0 = 2H_{inc} = \frac{4n_s}{(n_s+1)Z_0}E_0$, where n_s is index of refraction of substrate, Z_0 is the vacuum impedance and E_0=10 V/cm (Figure 2.7. (b)). The voltage developed across the gap due to induced current by incident pulse can be calculated by $V_{gap} = \frac{4twn_s}{\beta(1+4n_s)^2}E_0$, where t is the transmitted amplitude, $\beta = w/p$ is the coverage ratio, w is the gap width, p is periodicity of nanotrench in the sample. The calculated voltage across the gap is presented in Figure 2.7. (b). At bending state of closable nanotrench, it has parallel R-C circuit. The voltage across the gap in the time domain is calculated to be

$$V_{gap}(t) = \frac{1}{C}\int_{-\infty}^{t} \exp(\frac{\tau - t}{RC}) . I_0(\tau) . d\tau \quad \text{---------- (2.1)}$$

Where R and C is the resistance and capacitance across the gap, respectively. $I_0(\tau)$ is the induced current. The respective frequency (f) domain equivalent equation is

$$V_{gap}(f) = X_{gap}(f) I_0(f) \quad \text{---------- (2.2)}$$

Where $X_{gap}(f) = \frac{1}{\frac{1}{R} - i.2\pi fc}$ is the gap impedance. As the sample is bent, the gap width in nanotrench decreases and hence changes the capacitance of the gap. At a particular bending condition, the resistance starts to flow across the gap, as the metal parts starts touching each other. Using the above equation, the measured transmitted pulse is fitted with two fitting parameter R and C, which are presented in black dashed lines in Figure 2.7. (b). From the figure, it can be seen that the THz transmitted pulse is fitted well. The extracted R and C values for each bending presented in Figure 2.8.

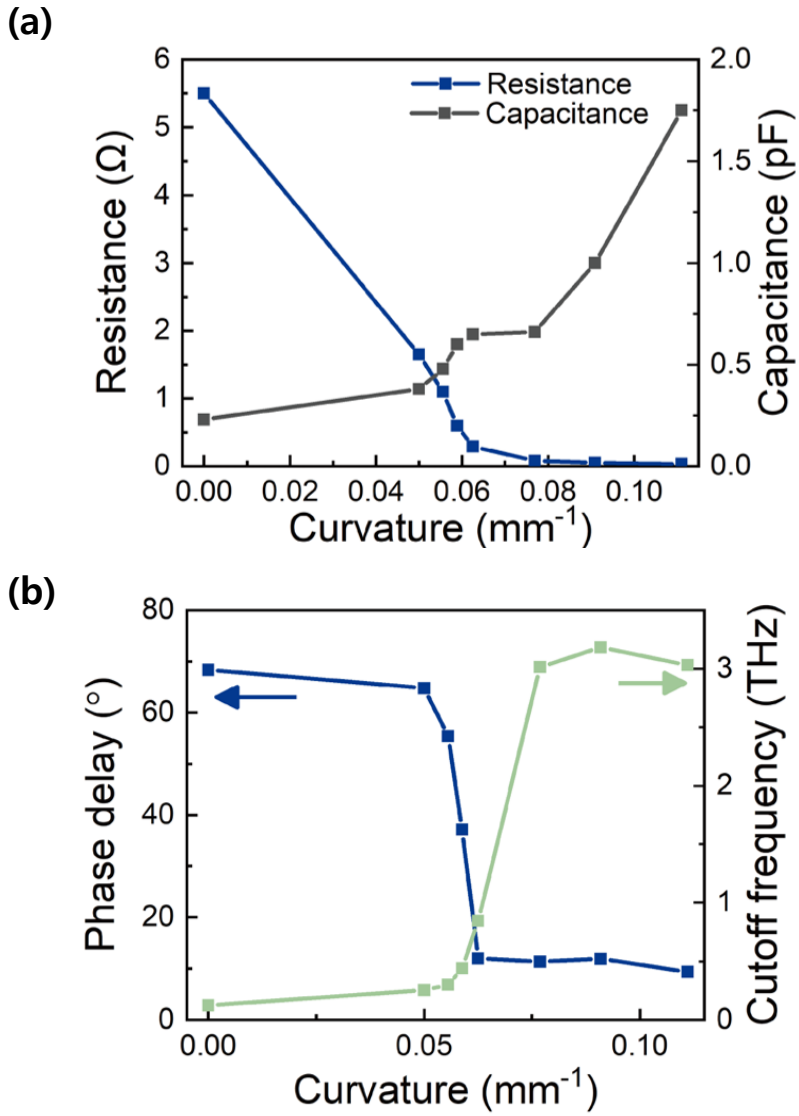

Figure 2.8. Extracted resistance and capacitance in closable nanotrench. (a) Extracted resistance and capacitance from THz transmitted pulse in closable nanotrench with respect to various bending state. (b) Experimental phase delay and cutoff frequency calculated from resistance and capacitance with respect to bending.

From Figure 2.8. (a), it is seen that the capacitance increases from 0.23 pF to 1.75 pF when the sample is bent from flat to bending radius curvature of 8 mm. Simultaneously, the resistance across the nanogap decreases drastically from 5.5 ohm to 0.03 ohm for the same bending conditions. The resistance and capacitance gives an insight about the gap closing mechanism and the reason behind the perfect extinction of the electromagnetic wave. From R and C, it is found that the gap impedance i.e. $\frac{1}{\frac{1}{R}-i.2\pi fc}$ drops as the sample is bent, which eventually screens the electromagnetic wave. This could also be seen from the phase data with respect to bending curvature as shown in Figure 2.8. (b). The phase changes from 70^0 to 5^0, as the sample is bent, showing that nanotrenches change from capacitive to conductive nature.

From plasmonics point of view, the effective dielectric constant of the gap is given by

$$\epsilon_{gap} = 1 + i\frac{1}{2\pi fRC} = 1 + i\frac{f_c}{f} \text{ ---------- (2.3)}$$

Where $f_c = \frac{1}{2\pi RC}$ is the cut-off frequency. The cut-off frequency vs curvature is presented in Figure 2.8. (b). With the help of the above equation, the mechanism for electromagnetism can be understood, which is presented schematically in Figure 2.9. When $f \gg f_c$, the screening in electromagnetic wave is primarily capacitive which directly related to overall gap width decrease (middle diagram, Figure 2.9.). For $f \ll f_c$, the capacitive charging is collapsed due to metal contacts (right side diagram, Figure 2.9.) and the screening of electromagnetic wave is dominated by conductance.

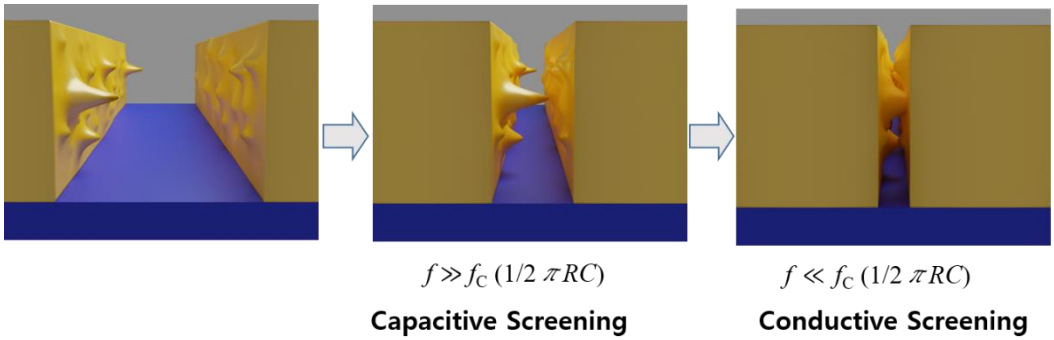

Figure 2.9. Mechanism explaining the electromagnetic screening in closable nanotrench. Initially, the screening is capacitive, which is due to gap width change (middle figure) and for higher bending, the conductive screening of electromagnetic wave dominates due to metal contacts (right side figure).

2.6. Applications of Closable Nanotrenches

After understanding the mechanism of electromagnetic screening mechanism in closable nanotrench sample, the application of this sample in various aspects is being explored. At first, a high density closable nanotrench sample was fabricated as earlier discussed fabrication technique [11, 13-14, 35]. The sample size is 20 mm by 20 mm containing long nanotrench of width 20 nm and 5 μm periodicity. Considering the wavelength of microwave and terahertz, the nanotrench density is very high.

Firstly, I explored the modulation of field enhancement. The field enhancement can be calculated from the total transmission normalized to the nanotrench coverage area. In order to calculate the coverage area of nanotrench for various bending, the calculated gap width from structural mechanics' simulation (Figure 2.6.) is considered. By using the transmitted amplitude in THz frequency and gap width calculation, the field enhancement is calculated which is presented in Figure 2.10. (a). At flat, the field enhancement is found out be 200 for high density nanogap and it is modulated to 5000 by bending. The sample modulation with respect to gap width is again confirmed by finite element model simulation. Considering gap width of 4.7, 2.6, 1.6 nm, the field enhancement modulates considerably as shown Figure 2.10. (b). This modulation of field enhancement would be useful for various other application such as sensing different size of molecule, nano-fluidics channel.

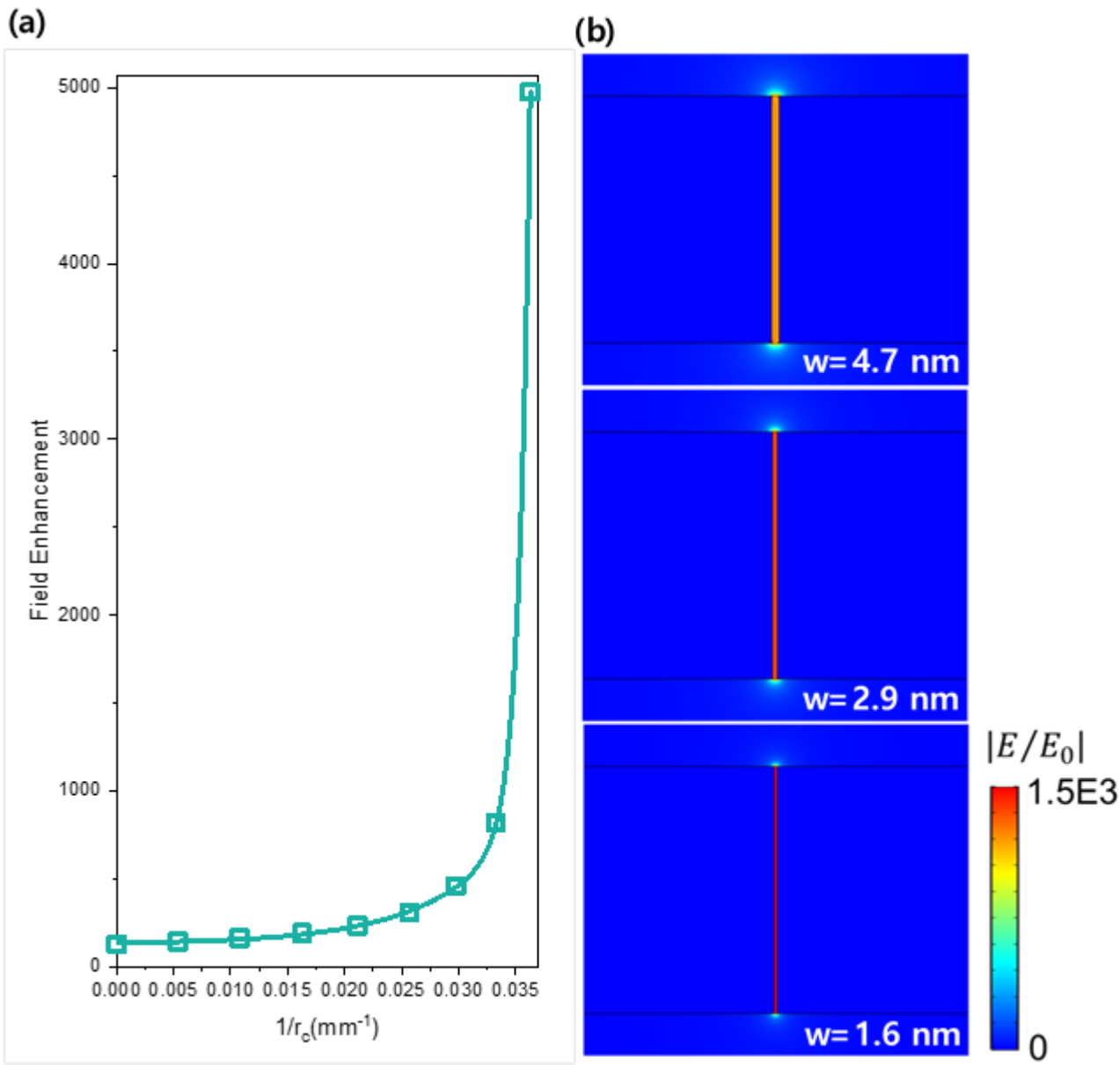

Figure 2.10. Modulation of field enhancement in closable nanotrench. (a) Field enhancement modulation in closable nanotrench for closable nanotrench with bending. (b) Simulation that confirms the enhancement of field enhancement with different gap width (w = 4.7, 2.9, 1.6 nm).

In second application, the same high density closable nanotrench sample is used for full modulation of electromagnetic wave at microwave frequency (at 15 GHz). FESEM image of the fabricated sample is shown in Figure 2.11 (a). The sample is inserted in the wave guide and exposed to successive bending strain and relaxation cycle while measuring the transmitted amplitude in real time. High density sample allow ~95% transmission at flat condition, which becomes zero for highest bending. Hence the sample could modulate the electromagnetic wave from full transmission to fully extinction mode just by strain as shown in Figure 2.11. (b).

Lastly, a direct application of the closable nanotrench is optical switch. For this application, I used an array of closable nanotrenches with 200 μm period, width 20 nm and height 150 nm. At flat, the nanotrench is opened and it allows optical light transmission fully as shown in Figure 2.12. (top figure). As the sample is bent, the intensity of the light starts decreasing as seen in the intermediator image in Figure 2.12. The sample finally blocked the light transmission for highest bending and hence it behaves like a switch.

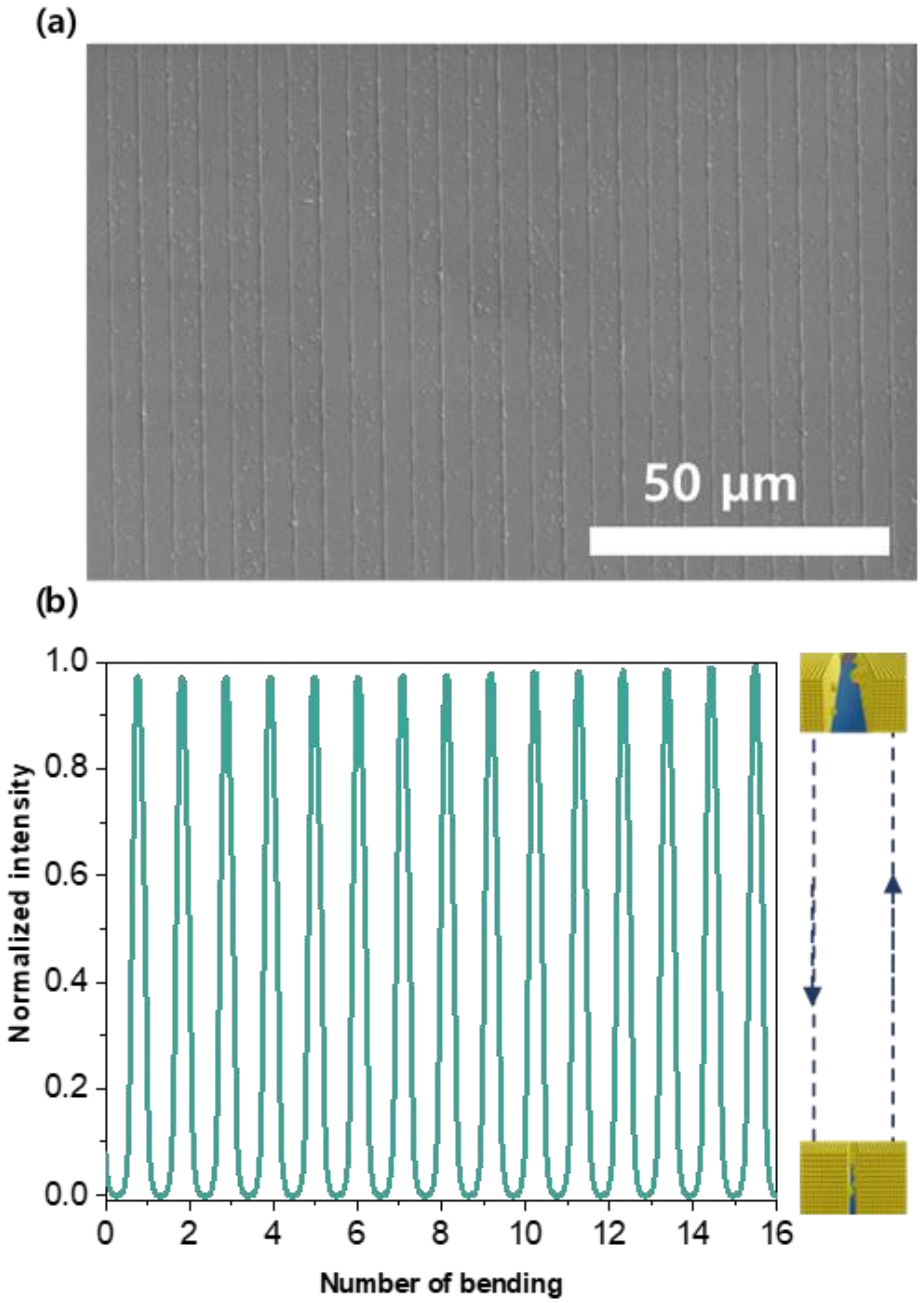

Figure 2.11. Full modulation of electromagnetic wave in high-density closable nanotrench. (a) FESEM image of high-density closable nanotrench. (b) Full-modulation of electromagnetic wave with bending.

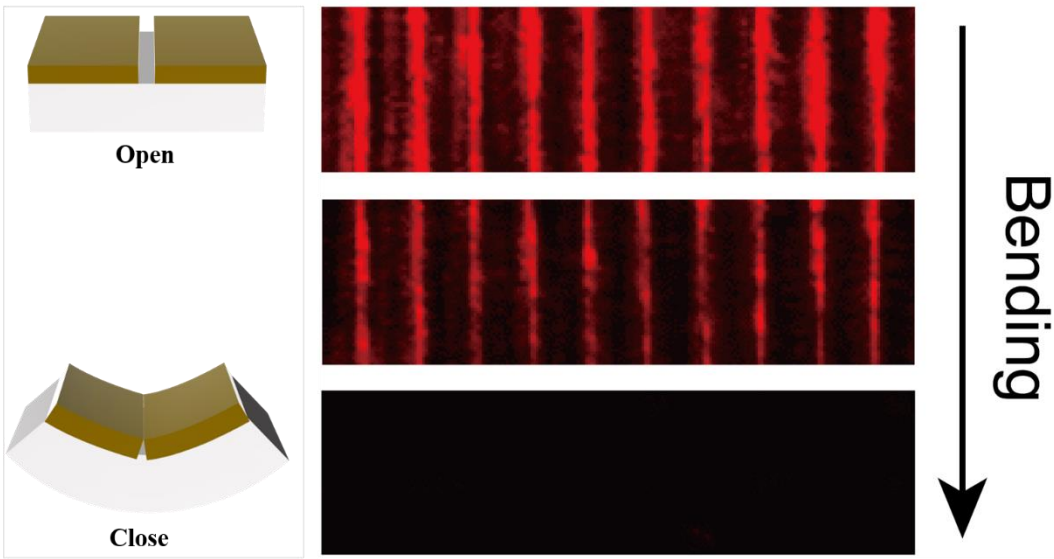

Figure 2.12. Optical switching in closable nanotrench. At flat, the closable nanotrench allow transmission of optical light (top picture) and the light is switched off (bottom picture) for highest bending, showing optical switch capabilities of the sample by bending.

2.7. Fatigue Test of Closable Nanotrench

For various application, the stability of closable nanotrench matters a great deal. Hence I tested the fatigue of the nanotrench. To investigate the fatigue, cycle of inward strain and relaxation is applied to the sample and simultaneously the microwave transmission at 15 GHz is measured in real time. The sample here used is the same high density closable nanotrench sample used in previous application in full modulation of electromagnetic wave. Initially, the sample behaves normally, having full modulation of microwave i.e. 95% to 0.01%. This behavior of full modulation sustains for about 200 times of bending and relaxation cycles. When the sample's bending and relaxation cycles exceeds 200, the functionality of the closable nanotrench

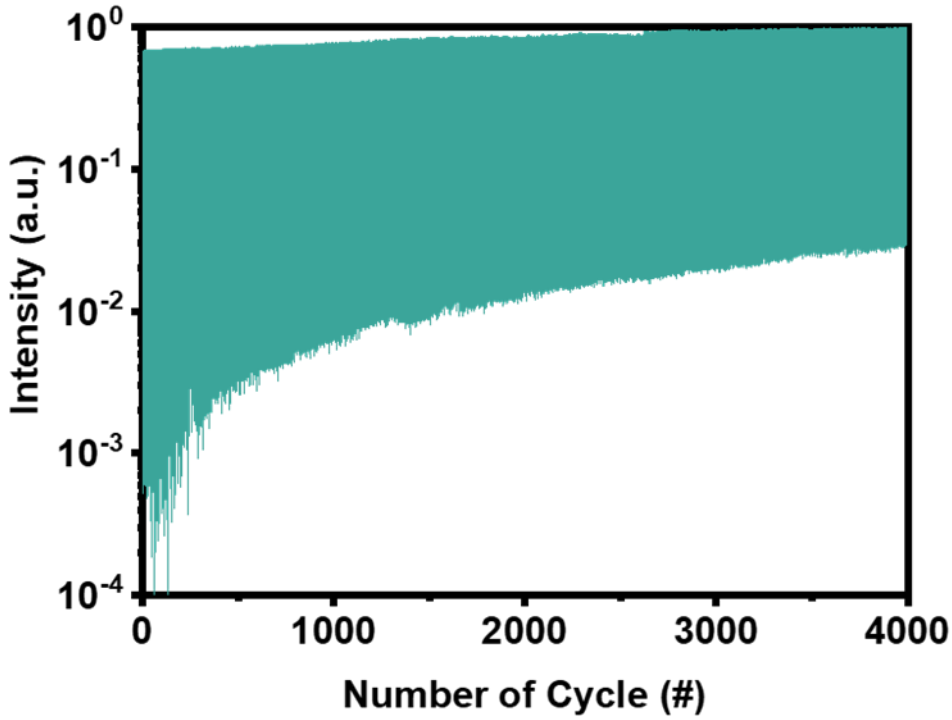

Figure 2.13. Fatigue test of closable nanotrench. The closable nanotrench is bent and relaxed in cycle for 4000 times. The sample shows good stability until 200 time bending cycle and then starts degrading.

Chapter 3.

Zero-Nanometer Gap Technology

3.1. Introduction

Metasurfaces have the ability to control optics in the subwavelength scale, showing unprecedented applications in optical components such waveplates, polarizers and lens. As discussed in chapter 1 and 2, metasurfaces ability can be enhanced if it can operate as an active device. These reconfigurable metasurfaces have drawn great interests among researchers recently and huge progress have been to improve the device quality [47-57]. However, still there are challenges to overcome in reconfigurable metasurfaces [58-59]. As can be observed from chapter 2, closable nanotrench have shown great functionality, showing full modulation of electromagnetic wave in almost all frequency regimes [44]. Fine tuning of the gap from 20 nm to zero-nanometer shows a huge change in the sample optical properties. From Figure 2.13. in chapter 2, it is seen the metallic nanotrench shows low stability and shows full functionality till 200 time of bending/relaxation cycles. Beyond 200 times, the sample shows significant degradation in microwave intensity modulation. To improve upon it, the best way could be starting from zero-nanometer gap and gradually open the gap so that we could start from minimum feature size smaller than state-of-the-art's limit.

In this chapter, a new kind of device or sample is fabricated, in which crack patterns are predefined on a flexible substrate. This sample with predefined crack patterns is called "zero-nanometer gap" or "zero-gap". A typical schematic diagram of zero-gap is presented in Figure 3.1. The zero-gap (top diagram of Figure 3.1.) is an interface between two metal

plates, deposited in two different conditions such as temperature and/or time. When the sample is bent in outward direction, a crack is formed at the interface, creating a metallic slot in between the metals as shown in the bottom picture of Figure 3.1. This fully connected metal to nanoslots in between metal allows to manipulate optics in a better way than nanotrench. The detailed fabrication process is discussed in the next section.

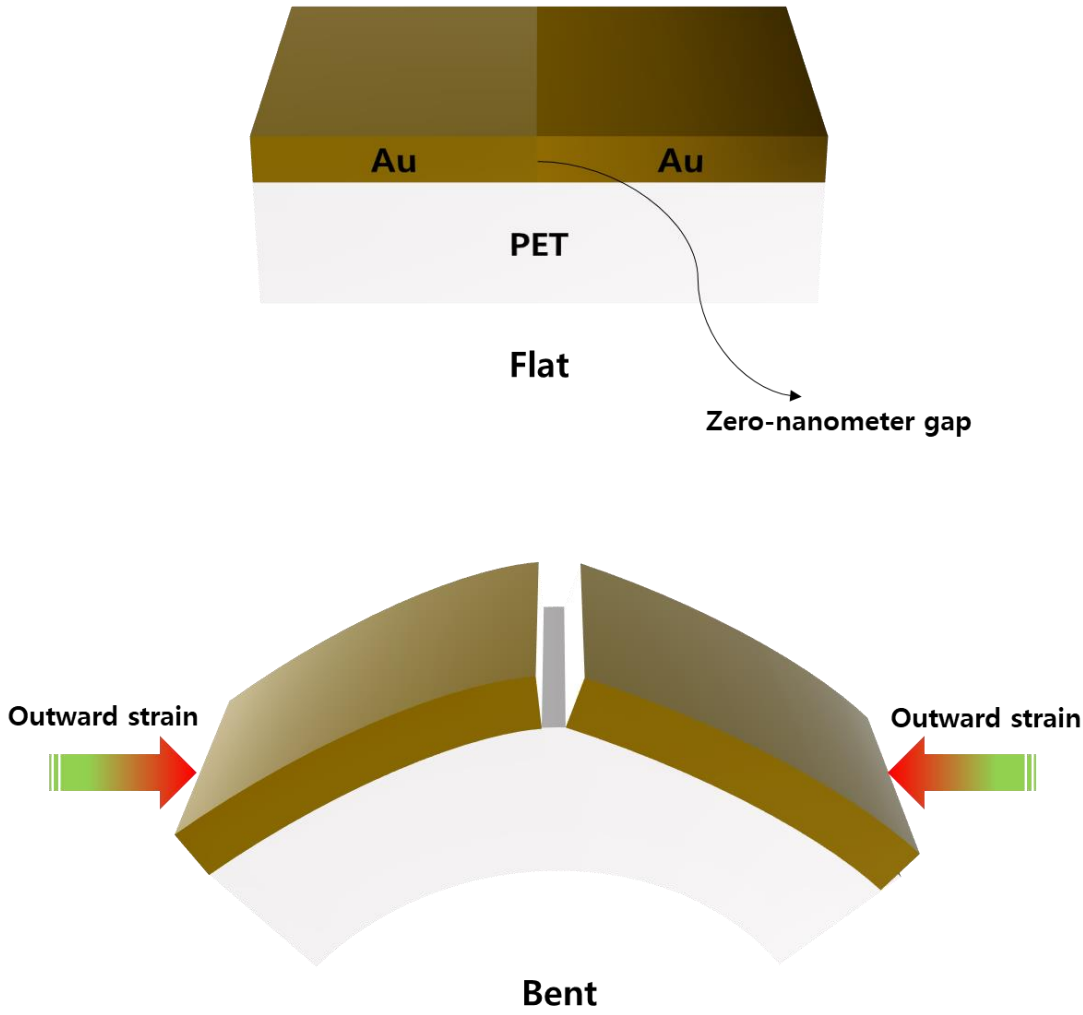

Figure 3.1. Schematic diagram of a zero-nanometer gap at flat and bent. Top diagram is the diagram of zerogap sample. At flat, there is no gap in the sample. The gap is formed in between two metal plates when the sample is bent.

3.2. Fabrication and Characterization of Zero-Nanometer Gap

The fabrication process, which is slightly different than closable nanotrench, is presented in Figure 3.2. Firstly, Polyethylene terephthalate (PET) substrate with dimension 20 mm by 20 mm is cleaned using in acetone and isopropanol in ultrasonic for 5 min each. The substrate is rinsed with deionized water and dried with N2 gas. Thin film of 3nm and 100 nm thickness of titanium (Ti) and gold (Au) respectively is deposited on the cleaned PET substrates with 0.5 A^{o}/sec by using E-beam evaporator. Photoresist patterning of desired dimension is done using typical photolithography and lift off process using image reversal resist AZ5214E. The details about this image reversal photolithography is described in chapter 2. A sacrificial mask is deposited on patterned photoresist pattern. Finally, the desired sacrificial mask patterning is fabricated by removing photoresist by acetone as shown in Figure 3.2. (a). The first layer of Ti/Au pattern is done by ion milling, shown in Figure 3.2. (b). Second thin film of 3 nm and 100 nm of titanium and gold respectively is deposited by evaporator with 1 A^{o}/sec (Figure 3.2. (c)). The excess metal layer is chemically etched to finally make the zero-nanometer gap sample (Figure 3.2. (d)). As seen from the schematic diagram (Figure 3.2. (d))), an interface is created in between two metal layer. This interface can be cracked open to have nanoslit in between the metal layer when the sample is exposed with outward strain (Figure 3.2. (e)).

The fabricated zero-nanometer gap is characterized by FESEM imaging, shown in Figure 3.3. This fabrication method enables to fabricate sample in wafer. Figure 3.3. (a) presents the digital image of zero-nanometer gap fabricated on 4-inch PET wafer. The sample contains an array of 20 mm long zero-gaps with periodicity 5 μm, height of 100 nm. The

periodic array of zero-gaps is shown in top view FESEM image in Figure 3.3. (b). The formation of the interface in between two metal plates deposited at two different conditions is confirmed by high magnified top view FESEM image, shown in Figure 3.3. (c). Cross-sectional FESEM image confirms the formation well defined interface between two metals with height of 100 nm.

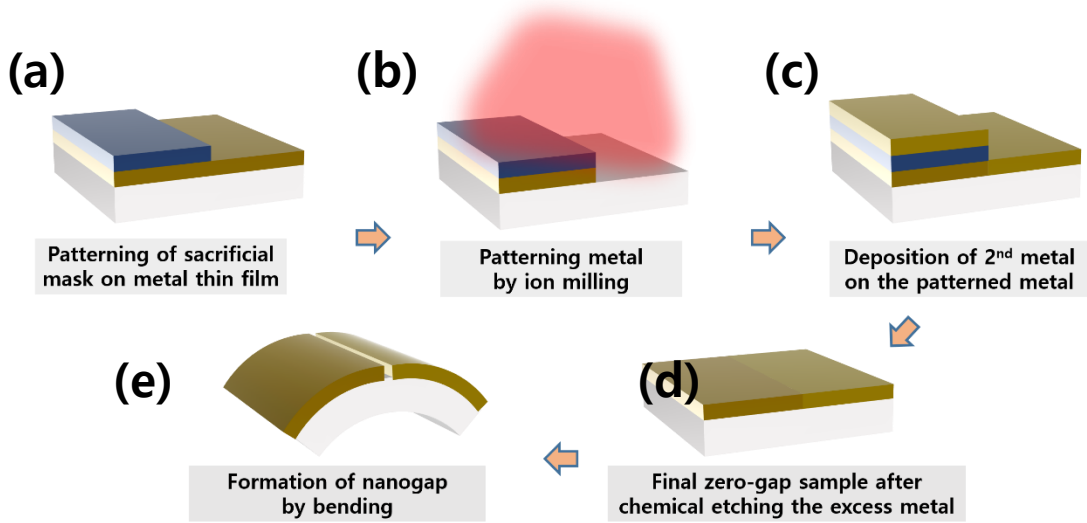

Figure 3.2. Fabrication process for zero-nanometer gap. (a) Patterning of sacrificial mask on titanium and gold thinfilm using photolithography and lift off process. (b) 1st layer metal pattern metal pattern by ion milling. (c) 2nd titanium and gold metal deposition using E-beam evaporator. (d) Fabricated zero-nanometer gap sample after etching the excess metal. (e) Nanoslit is cracked open at the interface between two metal layer by applying outward bend to the sample.

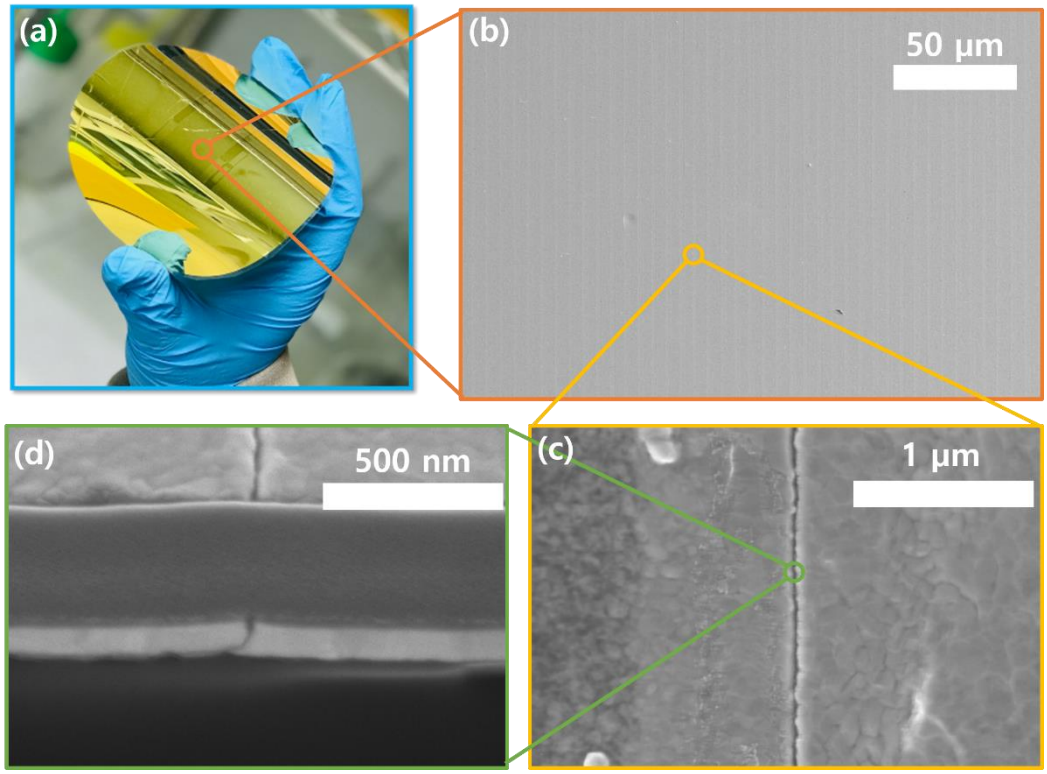

Figure 3.3. Characterization of Zero-Nanometer Gap. (a) Digital image of zero-nanometer gap samples fabricated on 4-inch PET wafer. (b) FESEM image of 5 μm periodic array of zero-nanogap-gap sample. (c) High magnified FESEM image of a zero-nanometer-gap showing the formation of interface between two metal plates. (d) Cross-sectional FESEM image of a zero-nanometer gap which shows formation of well-defined interface with height of 100 nm.

3.3. Functionality of Zero-Nanometer Gap

To check the functionality of zero-nanometer gap, at first I check the optical transmission through sample at flat condition and under outward strain. For this experiment, I use the same sample specification as mention in the previous section which is 5 μm periodic array of zero-gap with height 100 nm. Shown in Figure 3.3. (a) is the top view FESEM image of zero-nanometer gap at flat condition. At flat, the metal plates are attached fully. The optical transmission microscopy image Figure 3.3. (a) shows no transmitted light though the sample which again confirms that the interface is fully connected. In order to crack the interface, the sample is applied with outer bend strain. The strain opens a nanoslit by detaching the metal plates from each other. This gap opening i.e. nanoslit is observed by FESEM image in Figure 3.3. (b). The optical transmission microscopy image in Figure 3.3. (b) shows the full transmission of light through the gap area. The full light transmission means the nanoslit is formed perfectly when the sample is bent.

Secondly, the electrical conductivity is also checked the sample whether the metal plate is detached perfectly under outward strain. For this experiment, a metal micro-wire is fabricated in which it consists of single zero-gap. Shown in Figure 3.5. (a) is the schematic diagram of sample used to electrical conductivity across the zero-gap. The length of metal wire is 100 μm, containing a zero-nanometer gap of 20 μm long at the middle of the wire. The electrical conductivity (G_0) is measured across the zero-gap while sample is bent gradually [60-61]. The sample is started from flat and bent till 10 mm of radius of curvature. The conductivity across the gap vs curvature (inverse of radius of curvature) is presented

in Figure 3.5. (b). At flat, the metal plates are connected electrically and hence shows $300G_0$ (G_0 = 7.748 x 10^{-5} S is the conductance quantum). As the sample is bent, the conductance across the gap starts decreasing dramatically. Finally, the conductance becomes zero at around ~16.5 mm radius of curvature. This zero conductance confirms that the metal plates are fully detached from each other, creating a gap in the process. Again, the conductance is measured when the sample is relaxed by releasing the strain. The sample starts have the conductivity at 25 mm bending radius of curvature. The sample is able to regain the initial conductance of ~$300G_0$ when the sample is relaxed, showing the reconfigurable capability of the zero-nanometer gap sample (Figure 3.5. (b)).

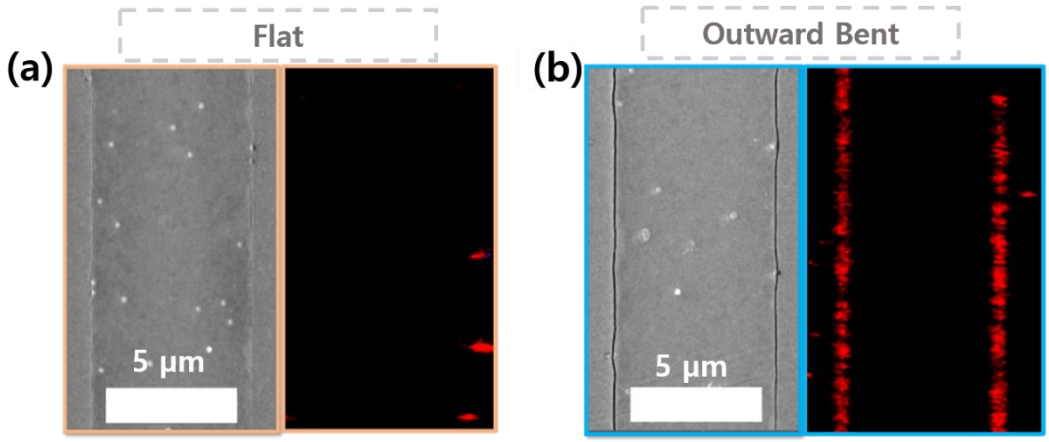

Figure 3.4. Functionality of zero-nanometer gap. Top view FESEM image and optical transmission through zero-nanometer gap at (a) Flat and (b) Outer bent condition.

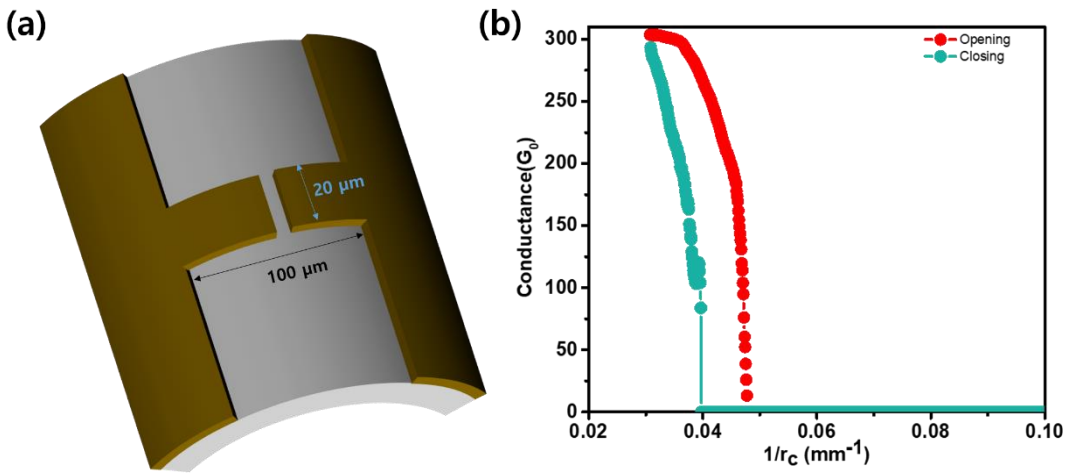

Figure 3.5. Conductance measurement across the zero-nanometer gap containing metal wire. (a) Schematic diagram of sample used for electrical conductivity measurement with respect to bending. The sample is the metallic wire (100 µm) containing single zero-gap with height of 20 µm and 100 nm thickness. (b) Measured electrical conductance across the zero-gap with bending radius of curvature. The conductance is express in the unit of quantum conductance "G_0" which is 7.748 x 10^{-5} S.

3.4. Electromagnetic Transmission in Zero-Nanometer Gap

Figure 3.6. represents the simulated optical properties of nanogap for different gap width. Periodic boundary condition with 5 μm periodicity with slits arrays (100 nm thickness) to replicate the actual sample specification for simulation. By bending the sample, it will reduce the periodicity and change the position of nanogap to the direction of propagation. However, these changes are very small as compared to microwave frequency and can be ignored while doing simulation. So the simulation of nanogap with different width is good enough to understand the functionality of zero-gap because with bending, the width of the zero-gap is essentially increasing. From Figure 3.6. (a-d), it can be seen that slit arrays can confine huge electric field and can also transmit huge amount of incident electromagnetic wave for perpendicular polarization with respect to long axis of the slits. Figure 3.6. (e) presents the transmitted amplitude with respect to a broad frequency range normalized with the periodicity of the sample in study which is P=5 μm. When the slits are far apart i.e. the periodicity is very high, the transmitted amplitude is inversely proportional to the frequency of the incident wave. When the slits are closely packed or highly dense i.e. the distance between the slits are very smaller than wavelength, it shows near unity transmission. From the graph, it can be seen that the sample attains ultra-broadband transparency for the wavelength range of 10^2-10^5 P [62-63]. The lower value of the wavelength is 300 μm, which corresponds to terahertz frequency. For zero-nanometer gap sample, I use microwave frequency with center frequency 15 GHz which is 2000 times the periodicity of the sample.

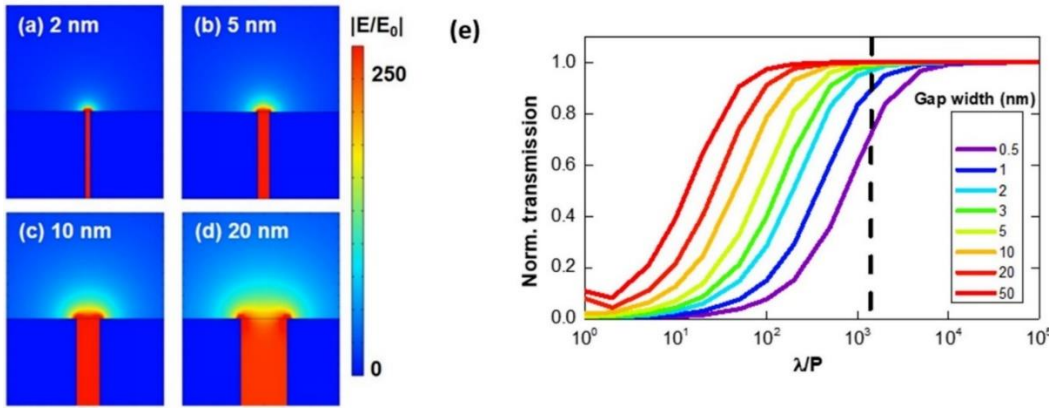

Figure 3.6. Simulation of optical properties of zerogap. (a-d) Distributions of electric field in the vicinity of the nanogap of different widths. (e) Far field transmitted amplitude in nanogaps of different gap width.

For this, the transmitted amplitude becomes more than 70% with only 0.5 nm of gap (Figure 3.6. (e)). This shows that huge change in the optical properties in the sample can be achieved with very small change in gap width, which will be useful for highly efficient switching operation.

After understanding from the simulation result, the sample's optical property is investigated in microwave frequency regimes (k_u band: 12-18 GHz) by using a vector network analyzer. The details of the microwave setup are explained in chapter 2 and Appendix 5.1. From the electrical measurement, it is found that at flat, the metals plates which are deposited at two different conditions are fully connected. In terms optics, this means that the sample will behave as a thin film on PET. To check this, 100 nm thick Au film is deposited on PET substrate by using E-beam evaporator. To compare the thinfilm and the zero-nanometer gap sample, the samples are inserted in between the waveguide pairs as shown in Figure 3.7. (a). The microwave (12-18 GHz) transmitted intensity for both the sample is presented in Figure 3.7. (b). This shows that the zero-nanometer gap sample behaves almost exactly as a thin film sample and transmits the microwave intensity of the same value as the thinfilm i.e. ~0.01%.

In order to check the functionality of zero-nanometer gap with bending, the sample is inserted in between waveguides pair with custom made sample holder with the ability to apply strain (See appendix and Figure 3.7. (a)). The sample is bent gradually from flat to 6.9 mm radius of curvature. As the sample is bent, the gap width increases from zero to ~100 nm. At flat, the sample transmits broadband microwave with intensity ~0.01% which

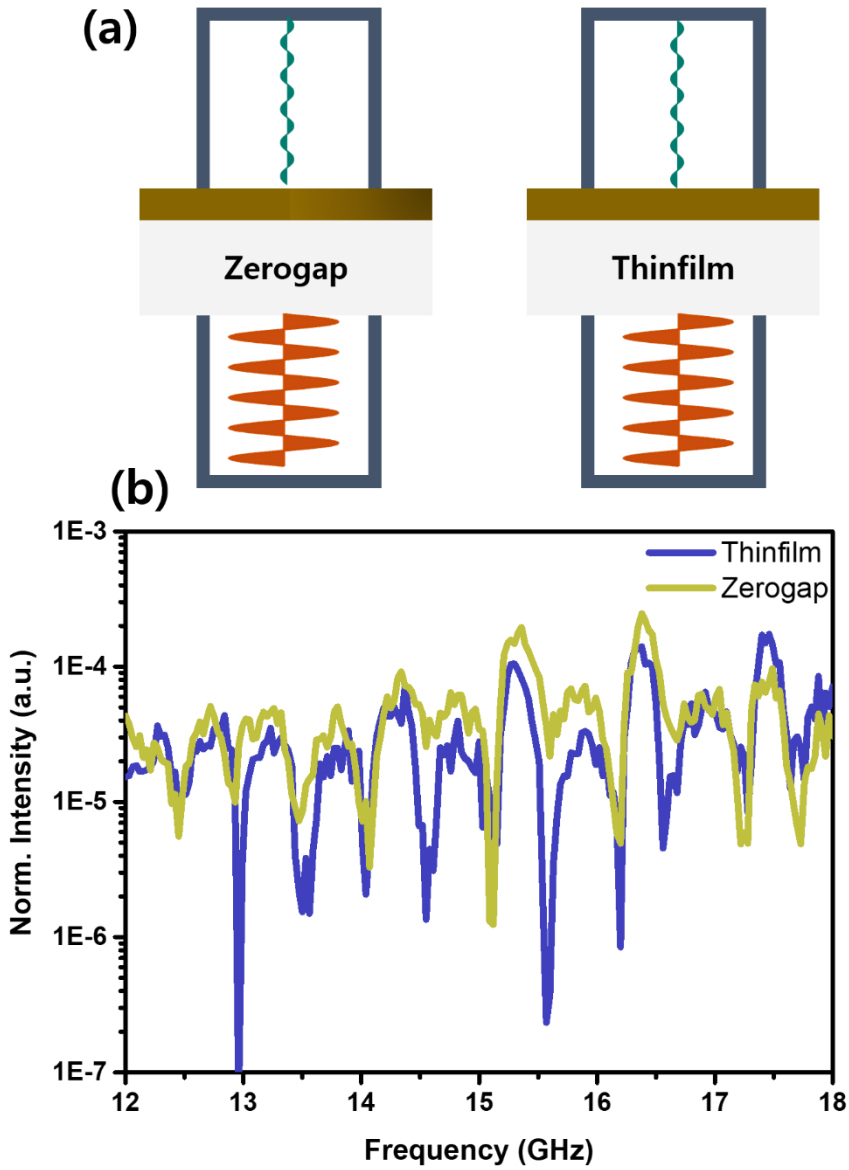

Figure 3.7. Microwave transmitted intensity through zero-nanometer gap and thin film. (a) Schematic diagram showing measurement scheme in microwave for zero-gap and Au thin film of thickness 100 nm. (b) Transmitted intensity for zero-gap and thin film in frequency range 12-18 GHz.

is direct transmission through a thin film. As the sample bent, the total transmitted intensity starts increasing and for highest bending, the sample transmits nearly 78% of microwave intensity. This shows that the sample has a modulation depth of $>10^4$. This microwave transparency at highest bending can be regarded as "on" state of the sample, whereas it can be considered as "off" at flat for perfect extinction of microwave intensity. This huge modulation of depth and absolute microwave transmission in broad frequency range are unprecedented when it comes to reconfigurable metamaterials. Since the gaps are modulated from zero or fully attached to bigger gap, the modulation of depth can be repeatable as the default state is zerogap, where the perfect extinction occurs. Table 1.1 presents the comparison in modulation depth achieved in previous work and the current study.

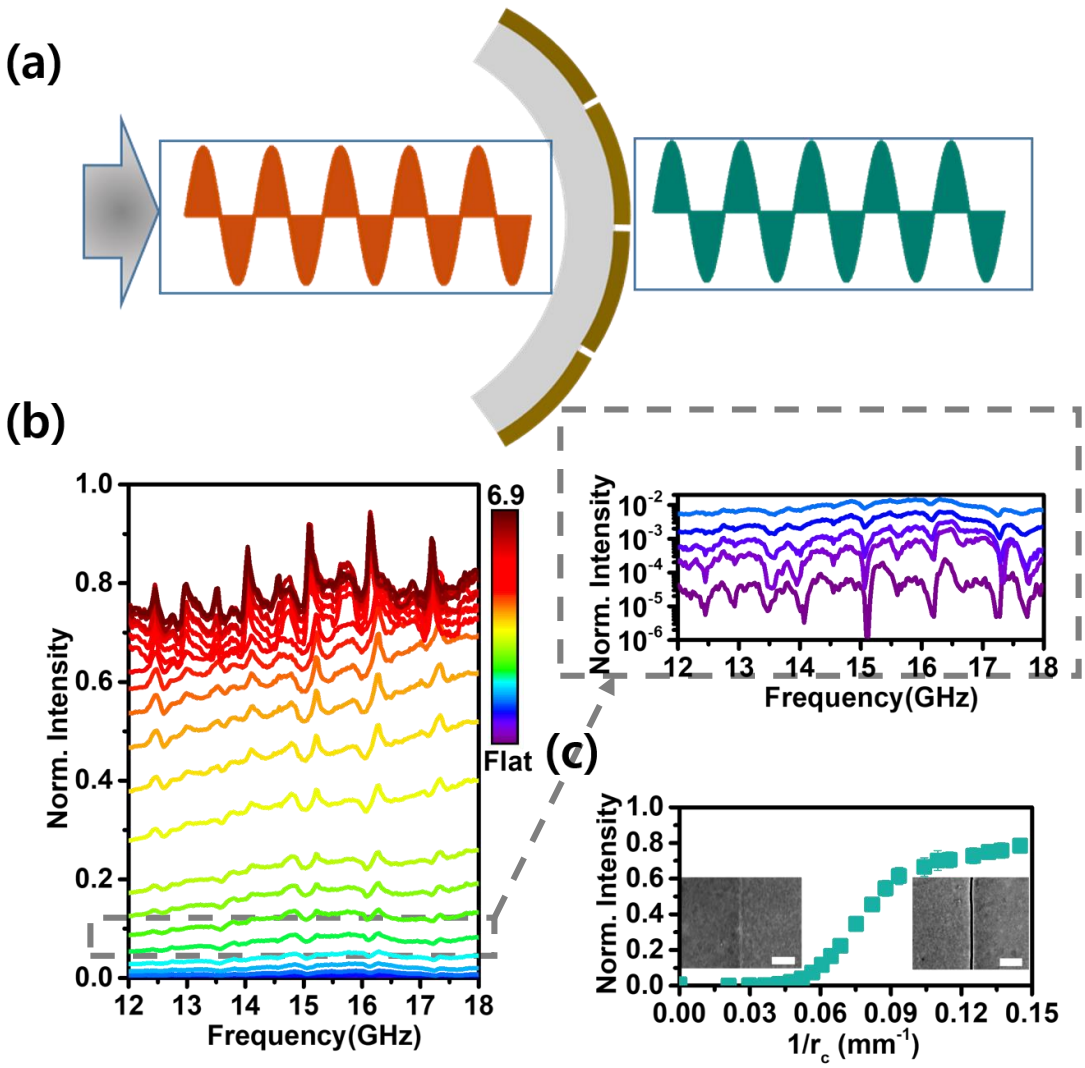

Figure 3.8. Microwave transmitted intensity through zero-nanometer gap with bending. (a) Schematic diagram explaining the measurement of microwave transmission with bending using a pair of waveguides. (b) Broadband microwave transmitted intensity through zero-gap with bending from flat to 6.9 mm radius of curvature. (c) Mean normalized microwave intensity vs curvature plot showing a huge modulation of depth offered by zero-nanometer gap.

Ref	External stimuli	I_max[a,b]	I_min[a,b]	I_max/I_min	Wavelength	Broadband?
64	Flexible substrate	70%	10%	7	Visible	No
65	Electro-mechanic	80%	5%	16	2 μm	No
66	Optical excitation	20%	2.5%	8	400 μm	No
67	Phase-change material	12%	0.24%	50	600 μm	No
This Work	**Flexible substrate**	**78%**	**0.001%**	**78000**	**Microwave**	**Yes**

Table 1.1. Comparison between different reconfigurable metasurface. Comparison amonst different reconfigurable metamaterials. (a, b) Maximum/minimum intensity at on/off state, respectively.)

3.5. Applications of Zero-Nanometer Gap

The ability of zero-nanometer gap in which it can modulate its gap width from zero to nanogap of the order of 100 nm may find various practical applications in future Here I investigated the application in transformative metasurface, modulation of electromagnetic from opaque to full transparency and modulation of field enhancement.

As observed in the previous experiments, the zero-nanometer gap blocks all the incidence electromagnetic wave at flat condition. When the sample is bent, nanoslits are formed at the interface between two metals. These nanoslits transmits electromagnetic wave polarized to the long axis and reflects the parallel polarized electromagnetic waves. Therefore, the zero-gap can be used as mirror when it is flat. It can also be used as a polarizer for bent condition. Due to this functionality, the zero-gap can transform from mirror to polarizer with just bending. Hence it has huge potential as "transformative metasurface". To realize the transformative metasurface functions of zero-nanometer, I follow the experimental methodology described schematically in Figure 3.9 (a) and (c). As seen from the diagrams, microwave transmitted intensity through zero-gap with respect to the angle between polarization and long axis is measured for both flat and bent condition. The corresponding result is presented in Figure 3.9. (b) and (d). At flat condition, the zero-nanometer shows the similar properties as a thinfilm. It means it reflects all the incidence electromagnetic wave incidence in different angle with respect to long axis of the interface. Thus it behaves as a mirror (Figure 3.9. (b)). When the sample is bent, the nanoslits are created by strain at the interface in between two metal. The nanoslits have the polarization

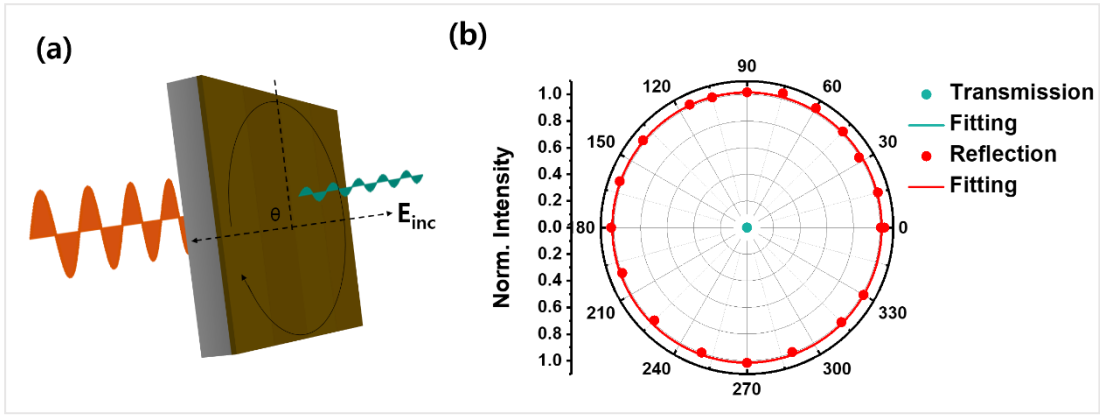

Figure 3.9. Zero-nanometer gap as transformative metasurface. Schematic diagram describing the angle dependence microwave intensity measurement scheme for (a) Flat, (c) Bent condition. (b) Reflected and transmitted microwave intensity through zero-nanometer gap at flat condition. In this situation, it reflects all the wave for all angle of incidence with respect to long axis. (d) Reflected and transmitted microwave intensity through zero-nanometer gap at bent condition. In this situation, it transmits all the wave and show good polarizability.

dependency. When the polarization is perpendicular to the long axis of the nanoslits, it transmits almost all the incidence microwave. However, as the sample is rotated, the angle between polarization and long axis changes and the intensity starts decreasing, following Malus's "$\cos^2\theta$" dependence. This demonstrates the polarizability of zero-nanometer gap when it is outer-bent. The transmitted ratio of this sample is found out to be $I_{on}/I_{off} > 7500$, which is comparable to commercial wire grid polarizer operating at mid-infrared frequency. Since the sample has zero-gaps packed densely. This high density gap transmits ~95% of microwave when it is bent as shown in Figure 3.8. (b). The real time modulation of microwave is presented in Figure 3.10. This shows a full modulation from 0.01% to ~95% in absolute value of microwave transmitted intensity with simple bending. Furthermore, the field enhancement modulation in zerogap with bending is also investigated. In order to calculate the field enhancement with bending, the change in gap width with respect to strain needs to be calculated first. This can be done by considering a simple geometry as shown in Figure 3.11. (a). At flat, let's assume "L" is the length of the sample. When the sample is bent, the top part of the sample expands, whereas the bottom part compresses. The neutral axis remains in its original length.

From geometry, $L = r_c\theta$ for neutral axis and For top layer, $L' = \left(r_c + \frac{h}{2}\right)\theta$

The gap width formed due to strain is $Ng = L' - L = \frac{h}{2}\theta = \frac{h}{2}\ \frac{L}{r_c}$

$$\Rightarrow g = \frac{hL}{2Nr_c} \text{ ---------- (3.1)}$$

Where as r_c is the radius of curvature, h is the thickness of PET, N is the ratio of total length to periodicity (P) of the zero-gaps i.e. L/P.

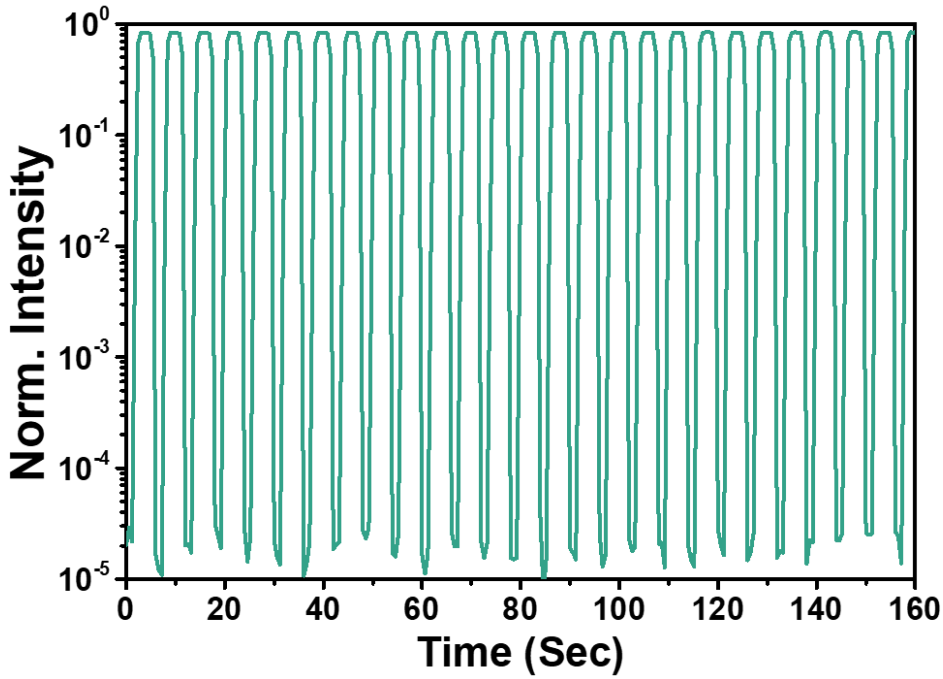

Figure 3.10. Full modulation of microwave intensity in zero-nanometer gap. The modulation of microwave intensity from 0.01% to 95% in zero-gap by bending.

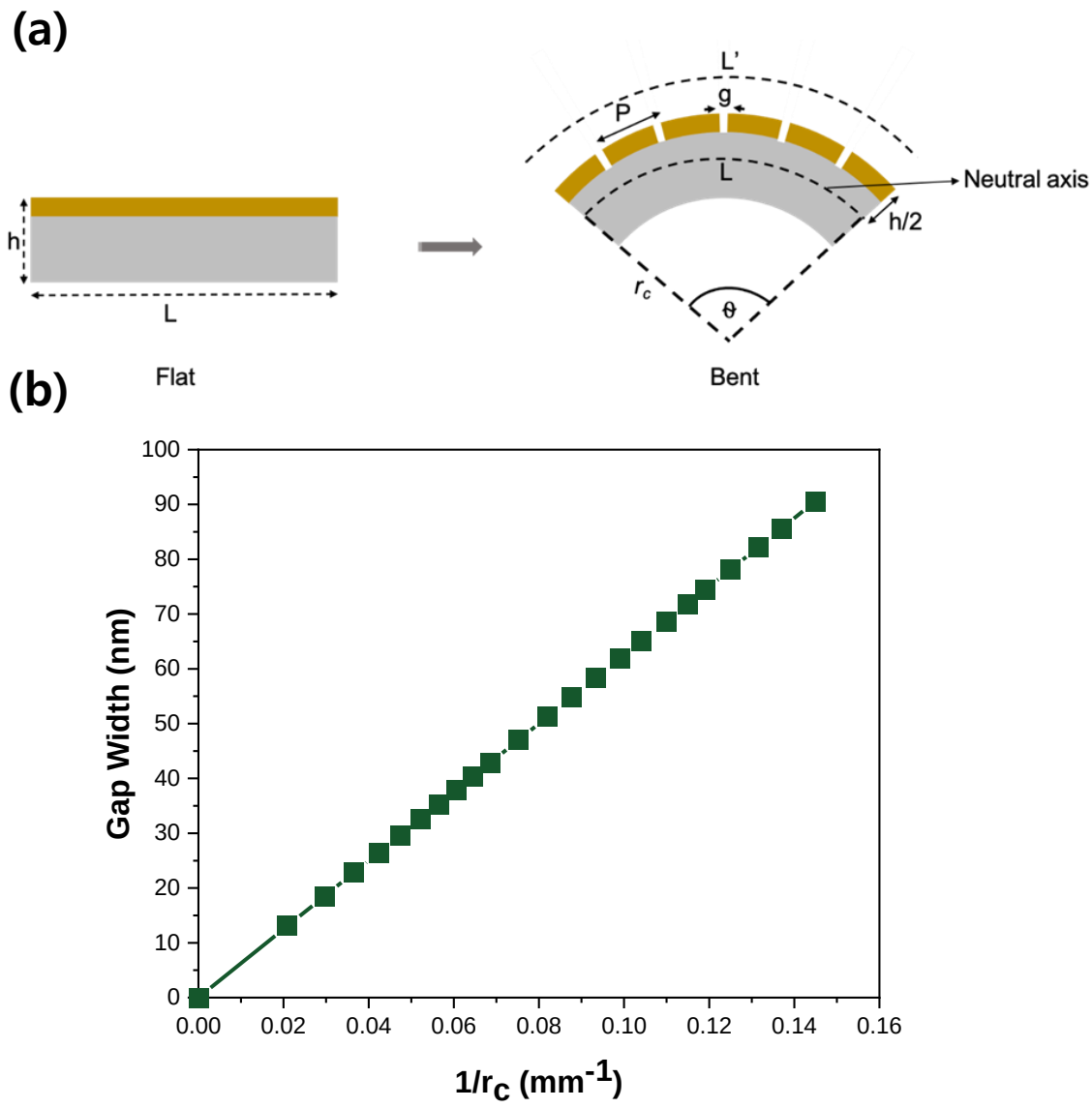

Figure 3.11. Calculation of gap-width in zero-gap with respect to bending of radius curvature. (a) Schematic diagraming describing the geometrical parameter for calculation of gap width with bending radius of curvature which is used for calculating field enhancement. (b) Modulation of gap width in zero-gap using bending radius of curvature.

The calculated change in gap width in zero-nanometer gap with respect to bending radius of curvature is calculated using the equation above and presented in Figure 3.11. (b). The gap-width is practically zero when the sample is at flat condition. As the sample is bent in outward direction, the metal plates starts to detach from each other by creating a gap width of the order of 100 nm. Note that the gap width changes linearly with curvature (inverse of bending radius of curvature), shown in Figure 3.11. (b). Now the field enhancement is the total transmission amplitude normalized with total coverage or area of the nanogaps. The coverage of nanogaps is calculated from the gap-width vs curvature data. The total transmitted amplitude in microwave is experimentally measured, shown in Figure 3.8. (c). Finally, the field enhancement with bending is calculated and presented in Figure 3.12. As observed in Figure 3.12., the field enhancement is modulated by bending the sample, which shows the functionality of the sample. Again, a direct application would be the modulation of transmission of light through zero-gap with bending. For this application, the sample is bent and relaxed successively while doing the optical transmission imaging. Figure 3.13. presents the optical transmission image in zero-gap with bending, showing high efficient switching of light.

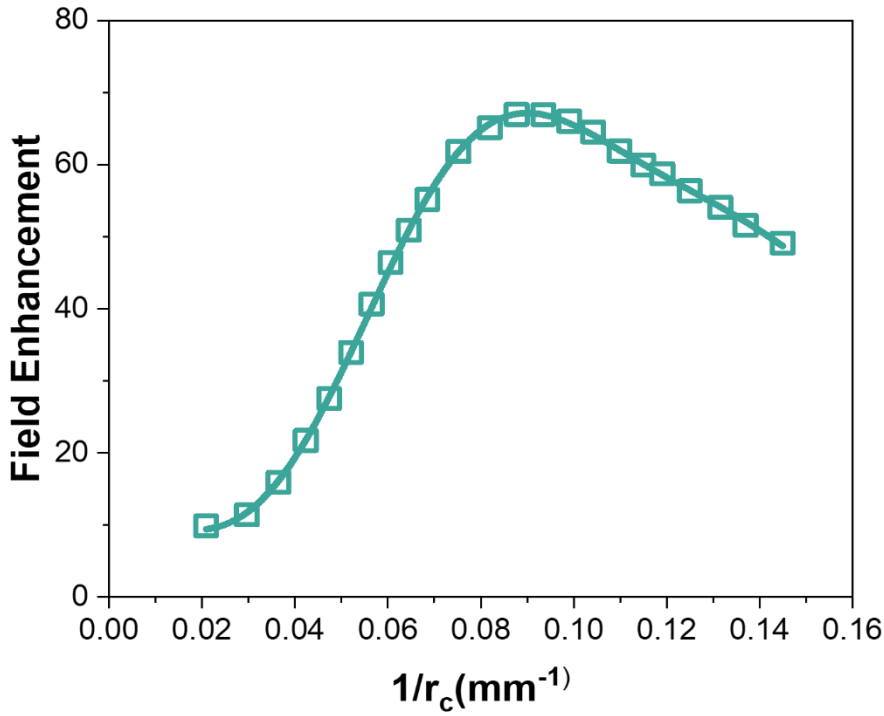

Figure 3.12. Modulation of field enhancement in zero-nanometer gap. Calculated field enhancement in zero-nanometer gap with curvature.

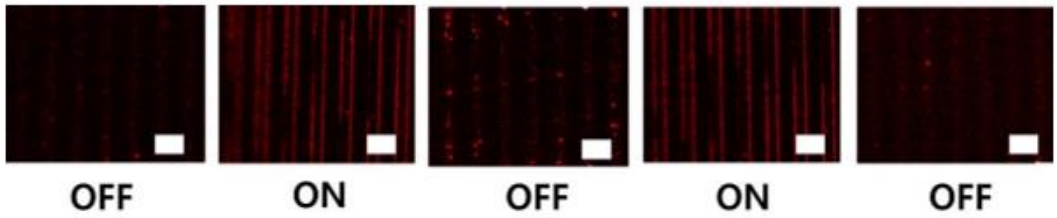

Figure 3.13. Optical switch in zero-nanometer gap. The optical transmission through zero-gap with bending, showing a good switching capabilities of zero-gap with bending (scale bar: 10 μm).

3.6. Fatigue Test of Zero-Nanometer Gap

For different application, especially in when it comes to industry, the stability of the sample to the external stimuli is an important factor. From the closable nanotrench's fatigue test, the sample could perform perfectly till 200 times. In the case of zero-nanometer gap sample, I tested the stability again. At first, I investigated the gap opening and closing mechanism in zero-gap sample by doing FESEM imaging in real time. Figure 3.14. (a) shows the FESEM images of zero-gap and nanogap formed with bending. It is observed that the gap can be created and destroyed with bending and relaxing the sample. This shows a good stability in gap opening and closing in the sample. Also, the sample is bent and relaxed continuously inside the waveguide, as the microwave intensity is measured. The sample is applied with the cycle of bending and relaxation for more than 10,000 times. From Figure 3.14. (b), it can be seen that the sample shows good stability over 10,000 times, which performs better than closable nanotrench (right side graph of Figure 3.14. (b)).

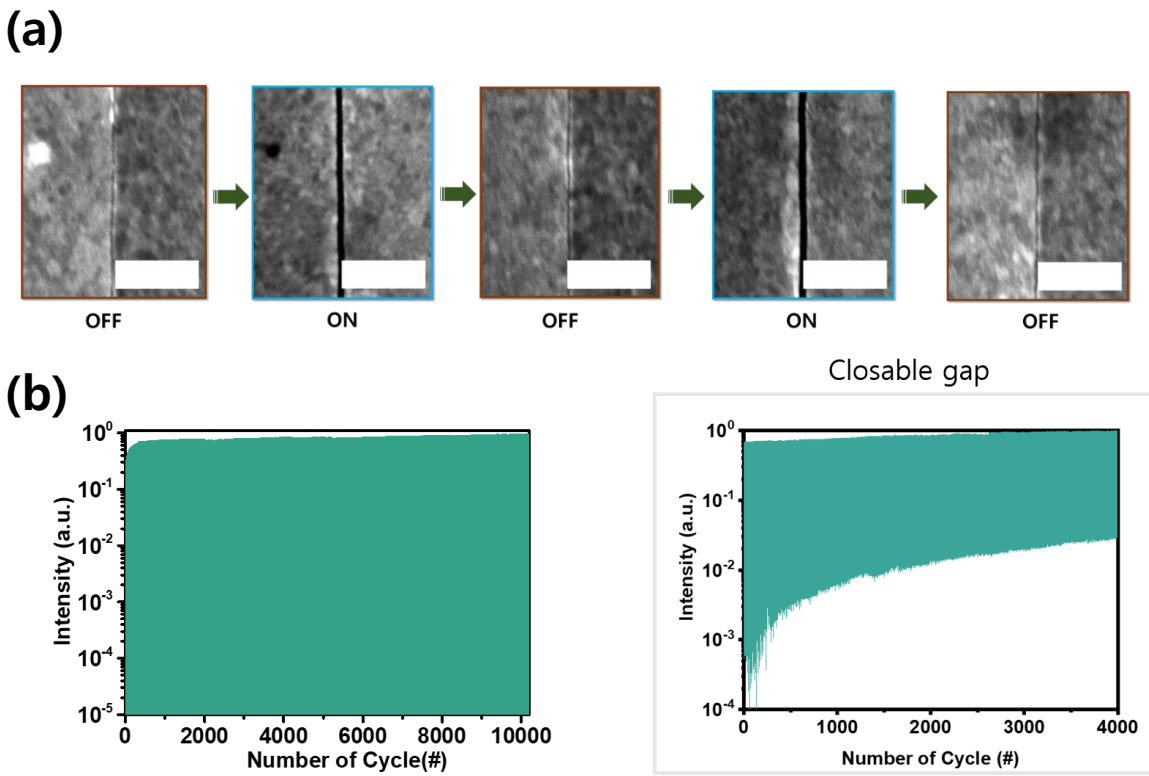

Figure 3.14. Fatigue test of zero-nanometer gap. (a) FESEM images of zero-gap and nanogap created in the same sample by successive bending of sample (1μm). (b) Microwave intensity modulation with respect to bending cycle of strain and relaxation for 10,000 times, showing a better stability with respect to closable nanotrench (shown in right side).

Chapter 4.

Conclusion and Future Work

4.1. Conclusion

To conclude, I fabricated two kinds of sample which are closable nanotrench and zero-nanometer gap sample. These two samples are fabricated on flexible substrates. By taking advantage of the flexible substrate, the sample's functionalities are investigated long wavelength and optical wavelength.

Closable nanotrench samples are fabricated on PET substrate using atomic layer lithography technique. Two samples containing nanoslits with periodicity 200 μm and 5 μm with height 150 nm of Au. Top view and cross-sectional FESEM images confirm the fabrication of good quality nanotrench in the sample. Closable nanotrench with periodicity 200 μm shows 50% of microwave transmitted amplitude at flat. With bending, the intensity becomes 0.1%, showing a perfect extinction of electromagnetic wave. This shows a subwavelength scale closing of the gap. Structural mechanics simulation of closable nanotrench is done to understand the closing mechanism of the nanotrench. It suggests the closable nanotrench under inward strain takes up tapered geometry in which metal edge at the top part touches each other, whereas the bottom part shrinks little bit. Furthermore, the gap width vs curvature data retrieved from the simulation suggests that the top part of the nanotrench closes faster than the bottom part. For highest bending, the width of the top part becomes zero, where the electromagnetic extinction occurs. To understand the closable nanotrench in terms of circuit theory and plasmonics, terahertz time domain

spectroscopy (THz-TDS) is done. At flat, the nanotrench shows 10% of transmits THz amplitude. The amplitude becomes almost zero with bending the sample till 9 mm of radius of curvature. This behavior of electromagnetic extinction is understood by using resistor-capacitor (R-C) modelling. The experimentally obtained time domain data for each bending radius of curvature are fitted with R-C circuit theory. Extracted R and C values with respect to radius of curvature of the sample suggest that at first the decrease in electromagnetic amplitude is due to the absolute change in gap width in the sample due to bending. At certain point, the metal starts touching each other and the current starts to flow across the nanotrench, thus achieving a perfect extinction of electromagnetic wave. With this understanding in hand, the closable nanotrench sample's ability is used for some application such as full modulation of electromagnetic wave in microwave frequency, modulation of field enhancement and optical switching using bending. For full modulation, high-density closable nanotrench is fabricated which shows modulation of wave from 90% to 0.1% of transmitted amplitude in real time. The fatigue test of the sample is also investigated which is useful for many practical applications. The sample is bent and relaxed for 4000 times while measuring the microwave transmission. The samples functionality remains constant till 200 times and then starts degrading suggesting the fatigue in the sample.

A concept of reconfigurable sample is conceived to improve upon this fatigue problem in closable nanotrench. This new concept of sample is called zero-nanometer gap, which is basically created by two metal plates, deposited at two different conditions using atomic layer lithography. In this work, the samples contain an array of zero-nanometer gaps with periodicity 5 μm and 100 nm height, made with Au metal. The fabrication of the sample is

confirmed by top view and cross-sectional FESEM imaging of zero-gaps. The sample at flat blocks all the microwave and behaves perfectly as a thin film of the same thickness. As the sample is bent, the gap opens up at the interface between the metal and starts transmitting microwave. The sample modulate microwave from 0.01% to 78% with outward bending. The gap opening with bending is corroborated with optical transmission image, FESEM image and conductivity measurement across the zero-gaps. I explore the zero-nanometer gap sample's functional ability as a "transformative metasurface". At flat, it reflects all the microwave intensity back for all the angle of incidence with respect to long axis, behaving perfectly as a mirror. With bending, the sample functions transformed to polarizer, in which it transmits light when the angle of incidence is perpendicular to long axis of gap and reflects all the light when the angle is parallel. Also, other application such as full modulation of electromagnetic wave and also field enhancement by changing the gap width, optical switching capabilities with bending is also shown. The fatigue test suggests the sample function perfectly for more than 10,000 times of bending and relaxation cycles with a modulation depth of 78000. With this unprecedented functionalities, these samples may find many practical applications in future.

4.2. Future Work

Closable nanotrench and zero-nanometer gap samples have shown unprecedented ability to control and manipulate the electromagnetic wave. However, from the real time measurement, it can be seen that the speed at which it modulates the wave is slow. Also, with bending of the sample, it's difficult to integrate the sample in various setup or systems. So it is apparent that there is room for improvement in the sample so that it can function in a faster way and easy to integrate with other systems or optical setups [68]. In this regard, zero-gap can be fabricated on top of a stretchable substrate such as PDMS instead of bendable substrate. However, its difficult to do nanofabrication on PDMS due to its surface properties. Here a transfer technique is used to fabricate zero-gaps on PDMS. The fabrication scheme is shown in Figure 4.1. With PDMS, the sample can be stretched and will show high modulation in much faster speed than that of the PET based zero-gaps. By controlling the PDMS thickness, the speed at which the modulation is done, could be changed. With very thin PDMS, it is possible to achieve kilohertz speed of modulation of electromagnetic wave.

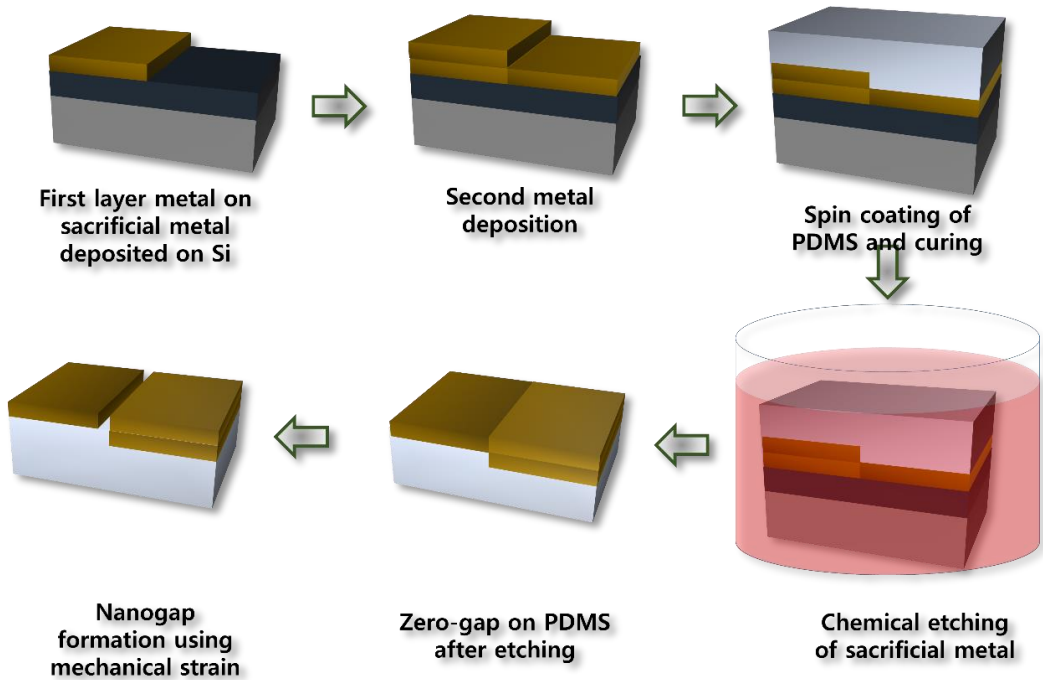

Figure 4.1. Schematic diagram of fabrication of zero-nanometer-gap on PDMS using transfer method. At first, the zero-gap is fabricated using atomic layer lithography on top of sacrificial layer/Si substrate. The PDMS is then spin-coated on the sample, followed by curing. The sample is finally detached from Si substrate by etching the sacrificial layer using chemical.

Chapter 5.

Appendix

5.1. Microwave Setup

The microwave transmitted intensity is measured using two open-ended waveguides, which is connected to vector network analyzer (E5063A), as shown in Figure 5.1. (a). The spot size of the waveguide (cross-section of waveguide) is 15.80 mm x 7.90 mm, shown in Figure 5.1. (b). The waveguide supports k_u band of microwave frequency which is 12-18 GHz. The waveguide also supports TE_{10} mode of the frequency band. Before measurement, waveguide pairs are calibrated using thru-reflect-line calibration technique. The sample inserted in between the waveguide pairs to measure the microwave transmission. The sample size is fabricated on 20 mm x 20 mm PET substrate to fit in the aperture of the waveguides. In order to measure the functionality of the sample, the sample is bent inside the waveguides while measuring the microwave transmitted intensity. This done by inserting the sample with custom made sample holder as shown in Figure 5.1. (c). The holder has the ability to apply strain to the sample with good precision, which is useful for calculating the value of radius of curvature with which the sample is bent.

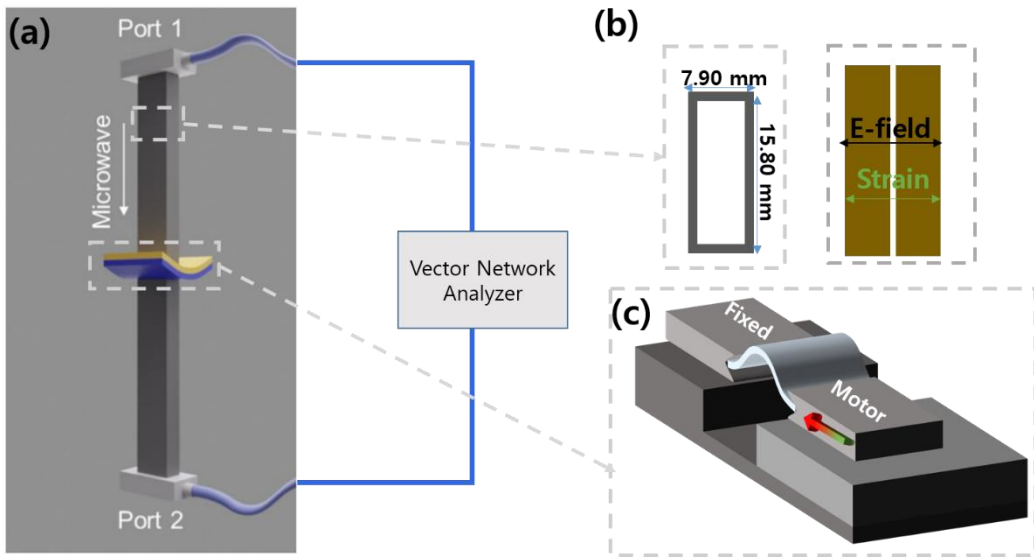

Figure 5.1. Microwave setup. (a) Schematic diagram describing the setup used for microwave transmission through closable nanotrench or zero-nanometer gap with bending. (b) Schematic diagram showing the aperture size of the waveguide and polarization direction in the waveguide. (c) Schematic diagram of sample holder used to bend sample while measuring the microwave transmission.

5.2. Terahertz Time Domain Spectroscopy (THz-TDS)

The terahertz time domain spectroscopy setup used for measuring terahertz transmission amplitude is shown schematically in Figure 5.2. (a). Briefly, a pump laser of wavelength of 532 nm and power 4 watt is used to pump a Ti: Sapphire cavity [68]. It generates 130 fs pulsed laser of wavelength 800 nm with repetition rate of 80 MHz. This femtosecond beam is divided into two parts, out of which one part is used to pump a DC-biased low temperature grown GaAs emitter for generating terahertz wave. Another part is used to probe the generated terahertz beam. The terahertz pulse, generated by pump beam is collected and directed by off-axis parabolic mirror to focus on ZnTe crystal (shown in Figure 5.2. (a)). Finally, the signal is detected using electro-optic sampling (EO sampling) technique. The measured frequency domain signal is shown in Figure 5.2. (b), which is propagated in free-space. The frequency bandwidth of the signal is 0.1-3 THz with a spot size of ~2 mm at the focus of terahertz beam.

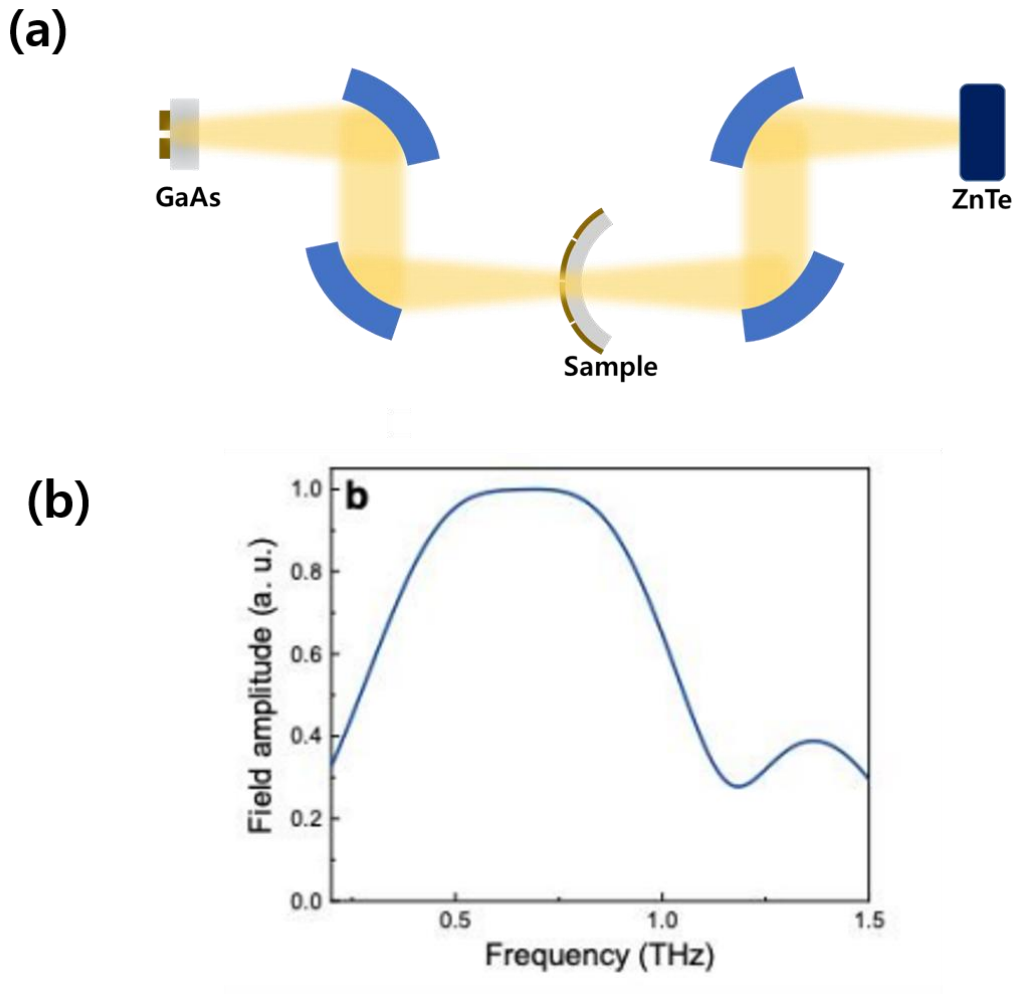

Figure 5.2. Terahertz Time-Domain Spectroscopy (THz-TDS). (a) Schematic diagram showing the setup of terahertz time domain spectroscopy setup used for terahertz transmission measurement. (b) Terahertz field amplitude in frequency domain measured in free-space.

5.3. Calculation of Radius of Curvature

One of the important parameter in this work is bending radius of curvature (r_c), which is used for different analysis. The general equation for radius of curvature is given by

$$r_c = \left|\frac{(1+y'^2)^{3/2}}{y''}\right| \qquad \text{------- (5.1)}$$

Where y represents the function at which the substrate is bent. In this case, the substrate bending curvature can be assumed to follow sinusoidal, as given below.

$$y = a \ \sin(kx) \qquad \text{------- (5.2)}$$

y and k are unknowns. These unknowns can be derived by using two constraints as below.

First constraint: The ends of the substrates are fixed in the stage.

$$y\ (x = 0) = y\ (x = L) = 0 \qquad \text{--- (5.3)}$$

Second constraint: The total length of the substrate doesn't change while bending.

$$l_0 = \int_0^l \sqrt{\left(1 + \left(\frac{dy}{dx}\right)^2\right)}\mathrm{dx} \qquad \text{------- (5.4)}$$

From equation (3), $k = {}^{\pi}/_{l}$

Equation (4) can also be written in a different form after integrating which is

$$l_0 = \left(\frac{2}{k}\right) \sqrt{1 + (ka)^2}.E\left(\frac{((ka)^2)}{(1+(ka)^2)}\right) \text{---- (5.5)}$$

Whereas E is the elliptical integral. By solving the above equation, a is obtained. With a and k in equation (2), the function of curve is expressed. This expression again inserted in equation (1) to finally get the equation for radius of curvature as given below.

$$\frac{1}{r_c} = \frac{ak^2 \sin kx}{(1+a^2k^2 \cos kx)^{3/2}} \quad \text{---- (5.6)}$$

5.4. Resistor-Capacitor Modeling

To describe the transmission of terahertz wave, the parallel resistor-capacitor (R-C) circuit is considered, which is shown schematically in Figure 5.3.

In this circuit, voltage across the gap can be calculated $V = q/C$, where q is the total charge accumulated in the capacitor C. Voltage related to resistance R is $V = I_R R$. I_R is the current flowing through resistance R.

The total current is given by $I_0 = I_R + \frac{dq}{dt}$ ------ (5.7)

This gives a differential equation for charge accumulation in the capacitor;

$$\frac{dq}{dt} + \frac{q(t)}{RC} = I_0(t) \quad \text{------ (5.8)}$$

After doing the Laplace transformation and using convolution theorem, the voltage across the gap can be expressed as

$$V_{gap}(t) = \frac{1}{C}\int_{-\infty}^{t} \exp\left(\frac{\tau - t}{RC}\right) . I_0(\tau) . d\tau \quad \text{------ (5.9)}$$

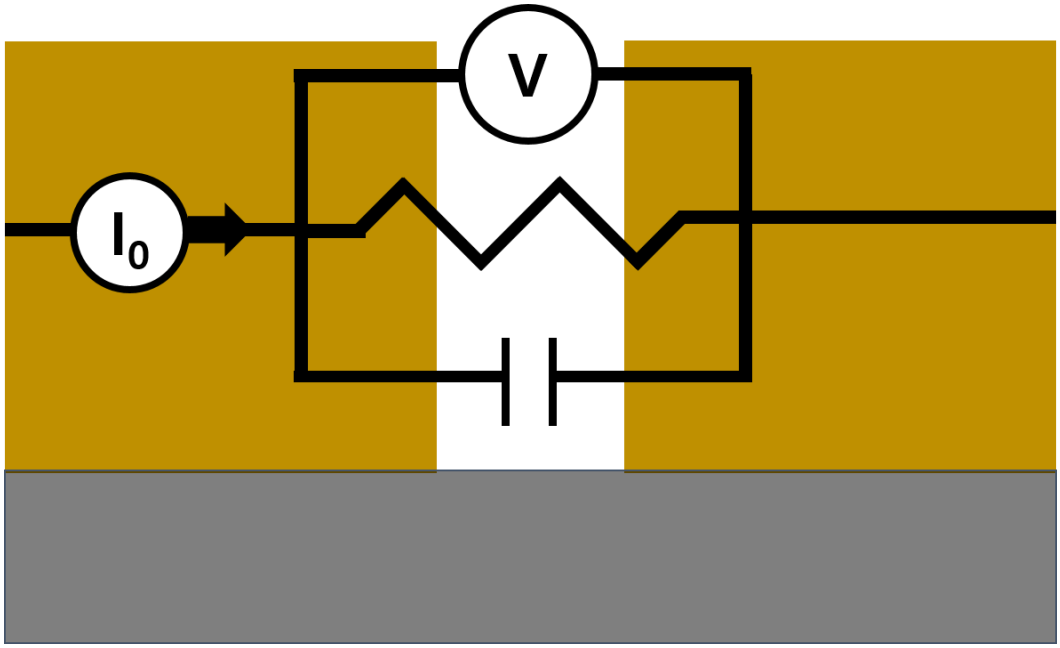

Figure 5.3. Resistor-Capacitor (R-C) Circuit Modeling.

Bibliography

[1] V. Sandoghdar, *Nano-Optics in 2020 ± 20*, Nano Lett. **20**, 4721 (2020).

[2] Q. Zhang, G. Hu, W. Ma, P. Li, A. Krasnok, R. Hillenbrand, A. Alù, and C.-W. Qiu, *Interface Nano-Optics with van Der Waals Polaritons*, Nature **597**, 187 (2021).

[3] S. Lal, S. Link, and N. J. Halas, *Nano-Optics from Sensing to Waveguiding*, Nat. Photonics **1**, 641 (2007).

[4] B. Du, Y. Yang, Y. Zhang, P. Jia, H. Ebendorff-Heidepriem, Y. Ruan, and D. Yang, *Enhancement of Extraordinary Optical Transmission and Sensing Performance through Coupling between Metal Nanohole and Nanoparticle Arrays*, J. Phys. D. Appl. Phys. **52**, 275201 (2019).

[5] S. G. Rodrigo, F. de León-Pérez, and L. Martín-Moreno, *Extraordinary Optical Transmission: Fundamentals and Applications*, Proc. IEEE **104**, 2288 (2016).

[6] C. Genet and T. W. Ebbesen, *Light in Tiny Holes*, Nature **445**, 39 (2007).

[7] T. W. Ebbesen, H. J. Lezec, H. F. Ghaemi, T. Thio, and P. A. Wolff, *Extraordinary Optical Transmission through Sub-Wavelength Hole Arrays*, Nature **391**, 667 (1998).

[8] H. Liu and P. Lalanne, *Microscopic Theory of the Extraordinary Optical Transmission*, Nature **452**, 728 (2008).

[9] F. J. García de Abajo, *Colloquium: Light Scattering by Particle and Hole Arrays*, Rev. Mod. Phys. **79**, 1267 (2007).

[10] M. A. Seo, H. R. Park, S. M. Koo, D. J. Park, J. H. Kang, O. K. Suwal, S. S. Choi, P. C. M. Planken, G. S. Park, N. K. Park, Q. H. Park, and D. S. Kim, *Terahertz Field Enhancement by a Metallic Nano Slit Operating beyond the Skin-Depth Limit*, Nat. Photonics **3**, 152 (2009).

[11] X. Chen, H.-R. Park, M. Pelton, X. Piao, N. C. Lindquist, H. Im, Y. J. Kim, J. S. Ahn, K. J. Ahn, N. Park, D.-S. Kim, and S.-H. Oh, *Atomic Layer Lithography of Wafer-Scale Nanogap Arrays for Extreme Confinement of Electromagnetic Waves*, Nat. Commun. **4**, 2361 (2013).

[12] D. Kim, J. Jeong, G. Choi, Y.-M. Bahk, T. Kang, D. Lee, B. Thusa, and D.-S. Kim, *Giant Field Enhancements in Ultrathin Nanoslots above 1 Terahertz*, ACS Photonics **5**, 1885 (2018).

[13] J.-H. Kang, D.-S. Kim, and M. Seo, *Terahertz Wave Interaction with Metallic Nanostructures*, Nanophotonics **7**, 763 (2018).

[14] Y.-M. Bahk, D. J. Park, and D.-S. Kim, *Terahertz Field Confinement and Enhancement in Various Sub-Wavelength Structures*, J. Appl. Phys. **126**, 120901 (2019).

[15] W. Park, J. Rhie, N. Y. Kim, S. Hong, and D.-S. Kim, *Sub-10 Nm Feature Chromium Photomasks for Contact Lithography Patterning of Square Metal Ring Arrays*, Sci. Rep. **6**, 23823 (2016).

[16] G. Choi, F. Shahzad, Y.-M. Bahk, Y. M. Jhon, H. Park, M. Alhabeb, B. Anasori, D.-S. Kim, C. M. Koo, Y. Gogotsi, and M. Seo, *Enhanced Terahertz Shielding of MXenes with Nano-Metamaterials*, Adv. Opt. Mater. **6**, 1701076 (2018).

[17] H.-R. Park, K. J. Ahn, S. Han, Y.-M. Bahk, N. Park, and D.-S. Kim, *Colossal Absorption of Molecules Inside Single Terahertz Nanoantennas*, Nano Lett. **13**, 1782 (2013).

[18] J. Rhie, S. J. Hong, D. Lee, D. Lee, H. S. Yun, Y.-M. Bahk, and D.-S. Kim, *Twofold Plasmonic Resonator Based on Polyethylene Terephthalate Thin Films for Terahertz Sensing Applications*, ACS Appl. Nano Mater. **4**, 8753 (2021).

[19] B. Das, H. S. Yun, N. Park, J. Jeong, and D.-S. Kim, *A Transformative Metasurface Based on Zerogap Embedded Template*, Adv. Opt. Mater. **9**, 2002164 (2021).

[20] K. Lee, J. Jeong, Y.-M. Bahk, J. Rhie, I.-K. Baek, B. J. Lee, Y. H. Kang, S. Hong, G.-S. Park, and D.-S. Kim, *Microwave Funneling through Sub-10 Nm Nanogaps*, ACS Photonics **3**, 537 (2016).

[21] Y.-M. Bahk, B. J. Kang, Y. S. Kim, J.-Y. Kim, W. T. Kim, T. Y. Kim, T. Kang, J. Rhie, S. Han, C.-H. Park, F. Rotermund, and D.-S. Kim, *Electromagnetic*

Saturation of Angstrom-Sized Quantum Barriers at Terahertz Frequencies, Phys. Rev. Lett. **115**, 125501 (2015).

[22] H.-T. Chen, W. J. Padilla, J. M. O. Zide, A. C. Gossard, A. J. Taylor, and R. D. Averitt, *Active Terahertz Metamaterial Devices*, Nature **444**, 597 (2006).

[23] F. Miyamaru, S. Hayashi, C. Otani, K. Kawase, Y. Ogawa, H. Yoshida, and E. Kato, *Terahertz Surface-Wave Resonant Sensor with a Metal Hole Array*, Opt. Lett. **31**, 1118 (2006).

[24] J. W. Lee, M. A. Seo, D. H. Kang, K. S. Khim, S. C. Jeoung, and D. S. Kim, *Terahertz Electromagnetic Wave Transmission through Random Arrays of Single Rectangular Holes and Slits in Thin Metallic Sheets*, Phys. Rev. Lett. **99**, 137401 (2007).

[25] N. Amer, W. C. Hurlbut, B. J. Norton, Y.-S. Lee, S. L. Etringer, and B. K. Paul, *Terahertz Wave Propagation in One-Dimensional Periodic Dielectrics*, Appl. Opt. **45**, 1857 (2006).

[26] J. W. Lee, M. A. Seo, D. J. Park, S. C. Jeoung, Q. H. Park, C. Lienau, and D. S. Kim, *Terahertz Transparency at Fabry-Perot Resonances of Periodic Slit Arrays in a Metal Plate: Experiment and Theory*, Opt. Express **14**, 12637 (2006).

[27] J. W. Lee, M. A. Seo, D. J. Park, D. S. Kim, S. C. Jeoung, C. Lienau, Q.-H. Park, and P. C. M. Planken, *Shape Resonance Omni-Directional Terahertz Filters with near-Unity Transmittance*, Opt. Express **14**, 1253 (2006).

[28] H. Kang, Q. Park, J. W. Lee, M. A. Seo, and D. S. Kim, *Perfect Transmission of THz Waves in Structured Metals*, JOURNAL-KOREAN Phys. Soc. **49**, 881 (2006).

[29] H. Cao and A. Nahata, *Resonantly Enhanced Transmission of Terahertz Radiation through a Periodic Array of Subwavelength Apertures*, Opt. Express **12**, 1004 (2004).

[30] S. Koo, M. S. Kumar, J. Shin, D. Kim, and N. Park, *Extraordinary Magnetic Field Enhancement with Metallic Nanowire: Role of Surface Impedance in Babinet's Principle for Sub-Skin-Depth Regime*, Phys. Rev. Lett. **103**, 263901 (2009).

[31] H. Tanoto, J. H. Teng, Q. Y. Wu, M. Sun, Z. N. Chen, S. A. Maier, B. Wang, C. C. Chum, G. Y. Si, A. J. Danner, and S. J. Chua, *Nano-Antenna in a Photoconductive Photomixer for Highly Efficient Continuous Wave Terahertz Emission*, Sci. Rep. **3**, 2824 (2013).

[32] Y.-M. Bahk, J.-W. Choi, J. Kyoung, H.-R. Park, K. J. Ahn, and D.-S. Kim, *Selective Enhanced Resonances of Two Asymmetric Terahertz Nano Resonators*, Opt. Express **20**, 25644 (2012).

[33] Y.-G. Jeong, Y.-M. Bahk, and D.-S. Kim, *Dynamic Terahertz Plasmonics Enabled by Phase-Change Materials*, Adv. Opt. Mater. **8**, 1900548 (2020).

[34] H. S. Yun, J. Jeong, D. Kim, and D.-S. Kim, *Active Thermal Control of 5 Nm Gap Terahertz Antennas*, Adv. Opt. Mater. **7**, 1800856 (2019).

[35] I. M. Pryce, K. Aydin, Y. A. Kelaita, R. M. Briggs, and H. A. Atwater, *Highly Strained Compliant Optical Metamaterials with Large Frequency Tunability*, Nano Lett. **10**, 4222 (2010).

[36] W. Liu, Y. Shen, G. Xiao, X. She, J. Wang, and C. Jin, *Mechanically Tunable Sub-10 Nm Metal Gap by Stretching PDMS Substrate*, Nanotechnology **28**, 75301 (2017).

[37] S. Xiao, T. Wang, T. Liu, C. Zhou, X. Jiang, and J. Zhang, *Active Metamaterials and Metadevices: A Review*, J. Phys. D. Appl. Phys. **53**, 503002 (2020).

[38] Y. Liu and X. Zhang, *Metamaterials: A New Frontier of Science and Technology*, Chem. Soc. Rev. **40**, 2494 (2011).

[39] V. G. Veselago, *THE ELECTRODYNAMICS OF SUBSTANCES WITH SIMULTANEOUSLY NEGATIVE VALUES OF ϵ AND μ*, Sov. Phys. Uspekhi **10**, 509 (1968).

[40] J. B. Pendry, A. J. Holden, W. J. Stewart, and I. Youngs, *Extremely Low Frequency Plasmons in Metallic Mesostructures*, Phys. Rev. Lett. **76**, 4773 (1996).

[41] J. B. Pendry, A. J. Holden, D. J. Robbins, and W. J. Stewart, *Magnetism from Conductors and Enhanced Nonlinear Phenomena*, IEEE Trans. Microw. Theory Tech. **47**, 2075 (1999).

[42] J. Jeong, J. Rhie, W. Jeon, C. S. Hwang, and D.-S. Kim, *High-Throughput Fabrication of Infinitely Long 10 Nm Slit Arrays for Terahertz Applications*, J. Infrared, Millimeter, Terahertz Waves **36**, 262 (2015).

[43] D. Kim, H. S. Yun, B. Das, J. Rhie, P. Vasa, Y.-I. Kim, S.-H. Choa, N. Park, D. Lee, Y.-M. Bahk, and D.-S. Kim, *Topology-Changing Broadband Metamaterials Enabled by Closable Nanotrenches*, Nano Lett. **21**, 4202 (2021).

[44] D. Grischkowsky, S. Keiding, M. van Exter, and C. Fattinger, *Far-Infrared Time-Domain Spectroscopy with Terahertz Beams of Dielectrics and Semiconductors*, J. Opt. Soc. Am. B **7**, 2006 (1990).

[45] Q. Wu and X. -C. Zhang, *Free-space Electro-optic Sampling of Terahertz Beams*, Appl. Phys. Lett. **67**, 3523 (1995).

[46] J.-Y. Kim, B. J. Kang, J. Park, Y.-M. Bahk, W. T. Kim, J. Rhie, H. Jeon, F. Rotermund, and D.-S. Kim, *Terahertz Quantum Plasmonics of Nanoslot Antennas in Nonlinear Regime*, Nano Lett. **15**, 6683 (2015).

[47] J.-Y. Kim, B. J. Kang, Y.-M. Bahk, Y. S. Kim, J. Park, W. T. Kim, J. Rhie, S. Han, H. Jeon, C.-H. Park, F. Rotermund, and D.-S. Kim, *Tunnelling Current-*

Voltage Characteristics of Angstrom Gaps Measured with Terahertz Time-Domain Spectroscopy, Sci. Rep. **6**, 29103 (2016).

[48] J. Guo, T. Wang, H. Zhao, X. Wang, S. Feng, P. Han, W. Sun, J. Ye, G. Situ, H.-T. Chen, and Y. Zhang, *Reconfigurable Terahertz Metasurface Pure Phase Holograms*, Adv. Opt. Mater. **7**, 1801696 (2019).

[49] J. Liao, S. Guo, L. Yuan, C. Ji, C. Huang, and X. Luo, *Independent Manipulation of Reflection Amplitude and Phase by a Single-Layer Reconfigurable Metasurface*, Adv. Opt. Mater. **n/a**, 2101551 (2021).

[50] G. Choi, T. K. Chau, S. J. Hong, D. Kim, S. H. Kim, D.-S. Kim, D. Suh, Y.-M. Bahk, and M. S. Jeong, *Augmented All-Optical Active Terahertz Device Using Graphene-Based Metasurface*, Adv. Opt. Mater. **9**, 2100462 (2021).

[51] W. Yang, K. Chen, Y. Zheng, W. Zhao, Q. Hu, K. Qu, T. Jiang, J. Zhao, and Y. Feng, *Angular-Adaptive Reconfigurable Spin-Locked Metasurface Retroreflector*, Adv. Sci. **8**, 2100885 (2021).

[52] Y. Nanfang, G. Patrice, K. M. A., A. Francesco, T. Jean-Philippe, C. Federico, and G. Zeno, *Light Propagation with Phase Discontinuities: Generalized Laws of Reflection and Refraction*, Science (80-.). **334**, 333 (2011).

[53] W. T. Chen, A. Y. Zhu, and F. Capasso, *Flat Optics with Dispersion-Engineered Metasurfaces*, Nat. Rev. Mater. **5**, 604 (2020).

[54] C. Pfeiffer, C. Zhang, V. Ray, L. J. Guo, and A. Grbic, *High Performance Bianisotropic Metasurfaces: Asymmetric Transmission of Light*, Phys. Rev. Lett. **113**, 23902 (2014).

[55] K. Mohammadreza, C. W. Ting, D. R. C., O. Jaewon, Z. A. Y., and C. Federico, *Metalenses at Visible Wavelengths: Diffraction-Limited Focusing and Subwavelength Resolution Imaging*, Science (80-.). **352**, 1190 (2016).

[56] B. Ratni, A. de Lustrac, G.-P. Piau, and S. N. Burokur, *Electronic Control of Linear-to-Circular Polarization Conversion Using a Reconfigurable Metasurface*, Appl. Phys. Lett. **111**, 214101 (2017).

[57] K. H. Nam, I. H. Park, and S. H. Ko, *Patterning by Controlled Cracking*, Nature **485**, 221 (2012).

[58] D. Kang, P. V Pikhitsa, Y. W. Choi, C. Lee, S. S. Shin, L. Piao, B. Park, K.-Y. Suh, T. Kim, and M. Choi, *Ultrasensitive Mechanical Crack-Based Sensor Inspired by the Spider Sensory System*, Nature **516**, 222 (2014).

[59] K. Yuki, S. Kurokawa, and A. Sakai, *Quantized Conductance in Pt Nanocontacts*, Jpn. J. Appl. Phys. **39**, 4593 (2000).

[60] Xu, He, and N. J. Tao, *Controlling the Conductance of Atomically Thin Metal Wires with Electrochemical Potential*, J. Am. Chem. Soc. **124**, 13568 (2002).

[61] H. R. Park, Y. M. Park, H. S. Kim, J. S. Kyoung, M. A. Seo, D. J. Park, Y. H. Ahn, K. J. Ahn, and D. S. Kim, *Terahertz Nanoresonators: Giant Field Enhancement and Ultrabroadband Performance*, Appl. Phys. Lett. **96**, 121106 (2010).

[62] Y. M. Bahk, H. R. Park, K. J. Ahn, H. S. Kim, Y. H. Ahn, D.-S. Kim, J. Bravo-Abad, L. Martin-Moreno, and F. J. Garcia-Vidal, *Anomalous Band Formation in Arrays of Terahertz Nanoresonators*, Phys. Rev. Lett. **106**, 13902 (2011).

[63] K. Fan and W. J. Padilla, *Dynamic Electromagnetic Metamaterials*, Mater. Today **18**, 39 (2015).

[64] D. Bouyge, A. Crunteanu, M. Durán-Sindreu, A. Pothier, P. Blondy, J. Bonache, J. Christophe Orlianges, and F. Martín, *Reconfigurable Split Rings Based on MEMS Switches and Their Application to Tunable Filters*, J. Opt. **14**, 114001 (2012).

[65] T. Kan, A. Isozaki, N. Kanda, N. Nemoto, K. Konishi, H. Takahashi, M. Kuwata-Gonokami, K. Matsumoto, and I. Shimoyama, *Enantiomeric Switching of Chiral Metamaterial for Terahertz Polarization Modulation Employing Vertically Deformable MEMS Spirals*, Nat. Commun. **6**, 8422 (2015).

[66] Z. Wang, L. Jing, K. Yao, Y. Yang, B. Zheng, C. M. Soukoulis, H. Chen, and Y. Liu, *Origami-Based Reconfigurable Metamaterials for Tunable Chirality*, Adv. Mater. **29**, 1700412 (2017).

[67] Y. Chen, Z. Shu, Z. Feng, L. Kong, Y. Liu, and H. Duan, *Reliable Patterning, Transfer Printing and Post-Assembly of Multiscale Adhesion-Free Metallic Structures for Nanogap Device Applications*, Adv. Funct. Mater. **30**, 2002549 (2020).

[68] J. Neu and C. A. Schmuttenmaer, *Tutorial: An Introduction to Terahertz Time Domain Spectroscopy (THz-TDS)*, J. Appl. Phys. **124**, 231101 (2018).

초록

나노홀, 나노슬릿, 나노다이머와 같은 금속 나노구조와 빛의 상호작용은 나노광학 분야의 주된 연구 대상입니다. 금속 나노구조에서 일어나는 강한 전자기장 증강은 금속 나노구조를 분자 감지를 위한 센서나 광학 부품 등 다양한 방면에서 활용할 수 있도록 합니다. 하지만, 금속 나노구조를 이용하여 빛을 능동적으로 조절하는 것은 도전적인 과제로 남아있습니다. 이 논문에서는 빛을 완전하게 조절할 수 있는 새로운 개념을 반영한 샘플을 제시합니다. 이것을 이용하면 하나의 샘플을 능동적으로 조작하는 것으로 전자기파를 완전히 투과시키거나 반대로 완전히 전자기파를 차폐할 수 있습니다. 원자층 증착 기술을 활용하여 유연성 기판 위에 클로저블 나노트렌치와 제로 나노미터 갭의 두 가지 형태로 샘플을 제작했습니다. 샘플을 유연성 기판 위에 제작하였기에 기계적인 변형을 가하는 것으로 투과 전자기파를 조절할 수 있습니다. 금속과 금속 사이에 공기 나노갭이 있는 구조의 클로저블 나노트렌치의 경우, 마이크로파 (12~18GHz) 및 테라헤르츠파 (0.2~2THz) 대역에서 안으로 굽히는 방향으로 힘을 가함으로써 투과를 극적으로 감소시킬 수 있습니다. 특히, 최대한으로 샘플을 굽혔을 때는 투과가 전혀 이뤄지지 않았는데, 이것은 갭 부분의 닫힘이 파장보다 작은 규모임을 나타냅니다. 이와 마찬가지로 고밀도의 클로저블 나노트렌지 샘플을 이용하면 마이크로파 투과를 완벽히 제어할 수 있음을 확인하였습니다. 한편, 제로 나노미터 갭 샘플을 바깥으로 굽히는 방향으로 힘을 가함으로써 빛의 투과를 0.01 %에서 75%까지 증가시켰습니다. 제로 나노미터 갭을 갖는 슬릿 구조에 힘을 가하여 거울을 편광판으로 바꿀 수 있음을 보였습니다.

키워드: 폐쇄형 나노트렌치, 제로 나노미터 갭, 테라헤르츠, 마이크로파, 변형 메타표면, 편광판

학생번호: 2016-39035

Acknowledgement

It would not have possible to finish doctoral degree without the support and help of many individuals. First of all, I would like to express gratitude towards my parents and brother for supporting throughout my life. I would like to thank my wife, Liza for all the support mentally and for giving the strength to carry on during my Ph.D. duration.

It is an honor to work under the supervision of Prof. Dai-Sik Kim, who helped me a great deal to improve on my research expertise and as a person too. I would like to thank him for that. Also, I would like to express my sincere thanks to all the individuals, involved with me during my Ph.D. time.